UPS19 modulates cancer cell migration and invasion and acts as a novel prognostic marker in patients with early breast cancer

Fabiana A Rossi [1,2]; Juliana H Enriqué Steinberg [1,2]; Ezequiel H Calvo Roitberg [1,2]; Molishree Joshi [3]; Ahwan Pandey [4,5]; Martin C Abba [6]; Beatrice Dufrusine [7]; Simonetta Buglioni [8]; Vincenzo De Laurenzi [7]; Gianluca Sala [7]; Rossano Lattanzio [7]; Joaquín M Espinosa [3,4,5] and Mario Rossi [1,2].

[1] Translational Medicine Research Institute (IIMT), Austral University, Pilar, Buenos Aires, Argentina.
[2] Biomedicine Research Institute of Buenos Aires (IBioBA-CONICET-MPSP), Capital Federal. Buenos Aires, Argentina.
[3]Functional Genomics Facility, University of Colorado School of Medicine, Aurora, Colorado, United States of America.
[4]Linda Crnic Institute for Down Syndrome, University of Colorado School of Medicine, Aurora, Colorado, United States of America.
[5]Department of Pharmacology, University of Colorado School of Medicine, Aurora, Colorado, United States of America.
[6]CINIBA-CONICET, Facultad de Ciencias Médicas - Universidad Nacional de La Plata, La Plata, Buenos Aires, Argentina.
[7]Department of Medical, Oral and Biotechnological Sciences, Center for Advanced Studies and Technology (CAST), 'G. d'Annunzio' University of Chieti-Pescara, Chieti, Chieti, Italy.
[8]Department of Pathology, Regina Elena Cancer Institute, Rome, Lacio, Italy.

Corresponding author: *Mario Rossi, Translational Medicine Research Institute (IIMT-CONICET), Austral University, Buenos Aires, Argentina. Av. Perón 1500, Pilar (zip code: B1629AHJ), Buenos Aires, Argentina. Email: mrossi-conicet@austral.edu.ar*

Running title: USP19 is a novel therapeutic target in breast cancer.

Keywords: USP19/invasion/breast/cancer/prognostic.

All authors have seen and approved the manuscript, and it hasn't been accepted or published elsewhere.

The authors declare no potential conflicts of interest.

ABSTRACT

Tumor cell dissemination in cancer patients is associated with a significant reduction in their survival and quality of life. The Ubiquitin-Proteasome System (UPS) plays a fundamental role in the maintenance of protein homeostasis both in normal and stressed conditions and its dysregulation has been associated with malignant transformation and invasive potential of tumor cells, thus highlighting its value as a potential therapeutic target. In order to identify novel molecular targets of tumor cell migration and invasion we performed a genetic screen with an shRNA library against UPS-related genes. To this end, we set up a protocol to specifically enrich positive migration regulator candidates. We identified the deubiquitinase USP19 and demonstrated that its silencing reduces the migratory and invasive potential of highly aggressive breast cancer cell lines. We extended our investigation *in vivo* and confirmed that mice injected with USP19 depleted cells display increased tumor-free survival, as well as a delay in the onset of the tumor formation and a significant reduction in the appearance of metastatic foci, indicating that tumor cell invasion and dissemination is impaired. In contrast, overexpression of USP19 increased cell invasiveness both *in vitro* and *in vivo*, further validating our findings. More importantly, we demonstrated that USP19 catalytic activity is important for the control of tumor cell migration and invasion. Finally, we showed that USP19 overexpression is a surrogate prognostic marker of distant relapse in patients with early breast cancer. Altogether, these findings demonstrate that USP19 might represent a novel therapeutic target in breast cancer.

INTRODUCTION

Cell migration plays a crucial role in a wide variety of physiological processes such as development, tissue injury and wound healing [1]. Its activation is highly regulated both spatially and temporarily, contributing to the maintenance of tissue and cellular homeostasis. Therefore, it is not surprising that when deregulated, migration is associated with the development and progress of multiple pathologies, including cancer [2-4].

During the development of malignant tumors, transformed cells change and acquire the ability to invade and abandon their original position. In order to do so, they need to pierce the surrounding extracellular matrix (invasion) and reach the circulatory torrent (intravasation). If they survive, some will be able to disseminate and get through distant capillary walls (extravasation), to invade the extracellular matrix in a new host environment, establishing a secondary tumor (colonization). During this process, cells acquire the ability to proliferate in an anchorage-independent manner with elevated invasive potential [5]. Cell motility plays a vital role in many of these events and therefore has a major influence in metastatic cell dissemination. Particularly in cancer, alteration or exacerbation of malignant tumor cell migration and dissemination is the principal cause of death due to solid tumors [6].

In addition, it was observed that decreasing the migratory capabilities of tumor cells can restore a certain level of sensitivity to cytotoxic reagents and increase the susceptibility to chemotherapeutic treatments [7, 8]. Consequently, targeting genes that regulate cell motility could be beneficial in the treatment of highly aggressive cancers [9, 10], and anti-migratory or anti-invasive activity is usually viewed as a desired attribute for novel anticancer drugs [11].

This complex process requires post-translational regulation of an innumerable amount of proteins, modifying their biological function, subcellular localization or half-life. Ubiquitination is an important form of protein post-translational modification that consists in the conjugation of ubiquitin polypeptides to target proteins. Ubiquitin tagged proteins are either subjected to destruction or responsible for regulating different processes, including endocytosis, DNA repair, cell cycle regulation, and gene expression [12]. The process of ubiquitin chain conjugation and elongation are regulated by a complex enzymatic cascade [13]. Also, like most post-translational modifications, the addition of poly-ubiquitin chains can be reversed or modified. This process is carried out by deubiquitinating enzymes (DUBs), a family of proteins including approximately 100 members classified into few sub-groups according to their catalytic core domains [14]. The ubiquitination cascade is of vital importance for the maintenance of cellular homeostasis by regulating a wide variety of processes, including cell migration and invasion [12, 15].

Therefore, within this framework, we conducted a loss-of-function genetic screen in order to identify novel molecular targets within the Ubiquitin-Proteasome System (UPS) that positively regulate migration. Screens targeting multiple genes significantly shortens experiment duration [16], and therefore they have been widely and successfully used to find genes involved in many physiological and pathological cellular processes [16-20], as they are relatively easy to perform and implement. In this study, we used a pooled shRNA interference library and an immortalized tumorigenic mammary epithelial cell line, MDAMB231, derived from a human triple-negative breast cancer. This type of cancer lacks expression of the estrogen receptor, progesterone receptor and human epidermal growth factor receptor 2 (HER2) and is associated with aggressive behavior and an overall poor prognosis [21]. Currently, there are no specific targeted therapeutic systemic alternatives for its treatment [22-24], and optimal chemotherapy regimens have yet to be established.

From our screen, we identified the Ubiquitin specific protease 19 (USP19) as a new candidate gene associated with the regulation of cell migration and invasion. This DUB is associated with protein quality control and cellular homeostasis [25-29].

To validate its novel function as a positive regulator of migration and invasion, we performed a series of *in vitro* and *in vivo* experiments analyzing USP19's role in colonization and tumor formation. In addition, we showed that USP19 overexpression is associated with distant relapse in patients diagnosed with early breast cancer (T1-2, N0, M0). Collectively, our data suggest that USP19 plays a crucial role in breast cancer cell dissemination, and we provide novel evidence that it can be a prognostic marker and attractive candidate for the development of new therapeutic strategies in breast cancer.

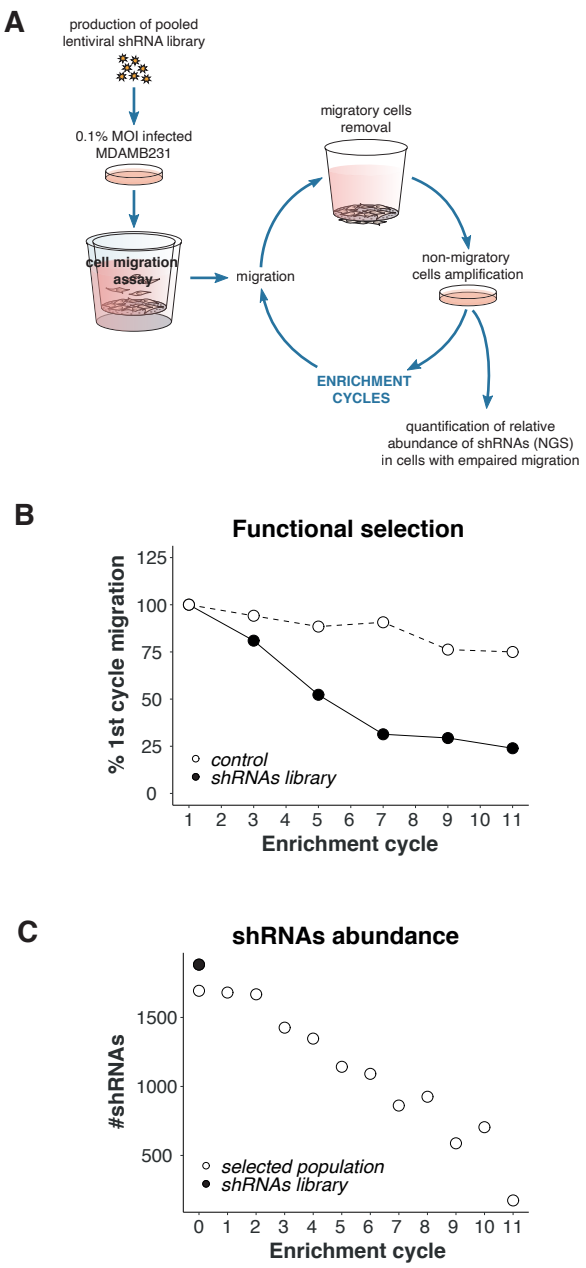

Figure 1| shRNA-based selection of positive regulators of cell migration.

(**A**) Overview of the selection procedure. The production and infection of a ubiquitination-related lentiviral shRNA library are described in Methods. Two weeks after lentiviral infection and selection, MDAMB231 cells were seeded onto transwell inserts and allowed to migrate across the porous membrane for 24 hours in order to select cells with a decreased migration phenotype. Migrating cells were removed and non-migrating cells were collected from the inserts upper compartment and amplified. Cells were then reseeded onto transwell culture inserts for a subsequent cycle of selection; this procedure was repeated until cells lost 80% of their initial migratory potential. After every cycle of selection, the relative abundance of the different shRNAs was evaluated using Next Generation Sequencing. (**B**) Transwell assay was used every other enrichment cycle to determine the percentage of migratory cells and monitor the selection process. (**C**) shRNAs' abundance was estimated after each selection cycle.

RESULTS

Migration-based screen to identify UPS genes with novel regulatory functions

In order to identify novel positive regulators of cell migration within the UPS, we performed an shRNA-based functional selection screen (Fig. 1A). A pooled recombinant lentiviral shRNA library targeting over 400 human UPS related genes (≈ 5 shRNAs per gene) was stably transduced into breast cancer cells. The functional selection consisted in placing the mixed population into the upper compartment of a transwell unit and allowing migration through the perforated membrane to the lower compartment. Cells that exhibited reduced migration were isolated from the upper compartment and amplified. We performed subsequent enrichment cycles until shRNA-transduced cells lost about 80% of their initial migratory potential (Fig. 1B). After every enrichment cycle, we evaluated shRNAs relative abundance in the cell population by PCR amplification and quantitative sequencing from genomic DNA. As shown in Figure 1C, as enrichment cycles increased, we observed a marked reduction in the number of shRNAs, suggesting that the selection process was efficient. As a control, we used an empty vector-transduced cell line.

Selection of candidate genes

After the selection process, we followed an analytical workflow to select candidate genes for further validation (Fig. 2A). In order to avoid false positives due to off-target effects, we discarded those genes for which only one shRNA targeting its sequence was found in the sequencing results. These criteria allowed us to identify 30 genes whose depletion impaired migration. Half of these genes had already been associated with migration, invasion, metastasis or tumorigenesis, and served as a proof of principle for the efficacy and specificity of our screen. Among the identified candidates, we focused our attention on the study of the deubiquitinase USP19.

Validation of USP19 as a regulator of cell migration

In order to validate USP19 as a potential regulator of cell migration, we established stable MDAMB231 cell lines transduced individually with two different shRNAs targeting USP19 expression,

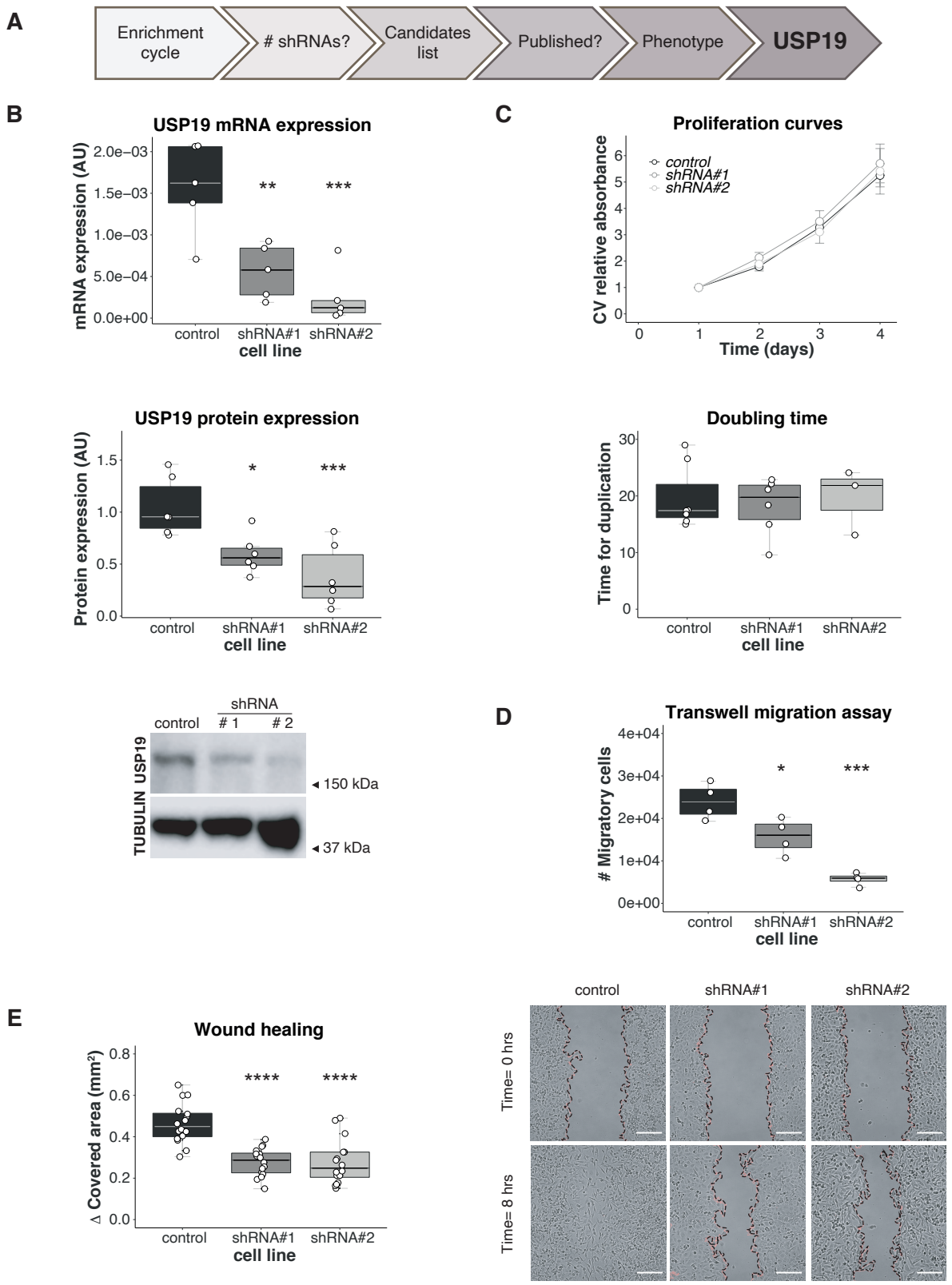

Figure 2| Validation and characterization of USP19 as a regulator of cell migration.

(**A**) Workflow used to select a candidate regulatory gene. MDAMB231 cells were stably transduced with control empty vector shRNA (control) or two different shRNAs (#1 & #2) targeting USP19. (**B**) Efficiencies of shRNA-mediated knockdown were confirmed by RT-PCR (top, n= 5, one-way ANOVA, Dunnett's multiple comparison test. shRNA#1 p= 0.0048 and shRNA#2 p= 0.0006) and Western Blotting (middle and bottom, n= 6, one-way ANOVA, Dunnett's multiple comparison test. shRNA#1 p= 0.0158 and shRNA#2 p= 0.0009). (**C**) Crystal violet (CV) staining was used to determine cell growth over time. Cells were seeded onto wells and allowed to attach. At the indicated time points, cells were fixed and then stained at the end of the experiment. The graph on the top shows the mean relative CV absorbance every 24 hours.

Doubling time was calculated for control and USP19 silenced cell lines on the bottom (n≥ 3, Kruskal-Wallis, Dunn's multiple comparison test. shRNA#1 p> 0.9999 and shRNA#2 p> 0.9999). Migratory potential was evaluated by two different experiments. (**D**) Transwell assay: After 24 hours of incubation, USP19-depleted cells were stained for microscopic examination and the number of migratory cells was compared to control cells. The graph shows the number of migratory cells per transwell membrane (n= 4, one-way ANOVA, Dunnett's multiple comparison test. shRNA#1 p= 0.0187 and shRNA#2 p= 0.0001). (**E**) Wound healing assays: scratching with a pipette tip made a gap on a monolayer of the different cell cultures, and time-lapse imaging monitored the number of migrating cells across the border. After 8 hours, cells exhibited different levels of migration. The graph on the left shows the gap covered area (mm^2) after 8 hours (n= 16, one-way ANOVA, Dunnett's multiple comparison test. shRNA#1 p< 0.0001 and shRNA#2 p< 0.0001) and the images on the right show representative areas in a wound healing experiment at the indicated time points. Scale bar= 100 µm.

named shRNA#1 and shRNA#2. Our results showed that both caused a significant reduction in USP19 mRNA and protein levels (Fig. 2B).

It is conceivable that shRNAs promoting cell proliferation may have also been enriched during the functional selection, as they gave the cells an advantage during the *in vitro* amplification step. To discard this possibility, we performed proliferation curves of control and USP19-silenced cell lines and calculated doubling rates. We observed no differences between the different cell lines (Fig. 2C, Supp. Fig. 1), providing evidence for a direct role of USP19 in the control of cell migration.

Next, to confirm the effect of USP19 depletion on cell motility, we used two independent assays: transwell migration and wound-healing assays. As shown in Figures 2D and 2E, USP19 knockdown significantly decreased the migratory potential of cells relative to the control cell line.

Altogether, these experiments indicate that USP19 silencing affects cell migration *in vitro*. We further confirmed our findings using another highly invasive breast cancer cell line (Supp. Fig. 2).

USP19 knockdown impairs invasion

Cell motility is often associated with increased tumor cell invasion and is a characteristic trait of aggressive tumor cells [30, 31]. Based on the observation that modulation of USP19 expression regulates migration, we decided to investigate the effect of USP19 depletion on tumor cell invasion.

To this end, we used three different experimental approaches. We first analyzed the ability of cells to invade agar spots. Our results show that USP19 knockdown significantly reduced the number of invading cells as well as their total displacement, compared to the control cell line (Fig. 3A).

We next performed a 3D growth assay by seeding cells at low confluence into noble agar, an anchorage-independent matrix. After 6 weeks in culture, the control cell line formed bigger colonies than USP19-silenced cell lines (Fig. 3B), indicating that colonization and matrix invasion in these conditions is partially impaired in cells where USP19 expression is reduced.

Finally, to further characterize USP19 depletion on tumor cell invasion, we assessed growth and invasion into a reconstituted extracellular matrix that provides anchorage (Matrigel®). Both cell lines expressing USP19 shRNAs showed colonies with a significantly smaller size than the control cell line (Fig. 3C), indicating that USP19 is required for efficient invasion even when anchorage is provided.

Similarly to the migration experiments, we further validated our results using another breast cancer cell line (Supp. Fig. 2).

Collectively, our results indicate that USP19 knockdown inhibits MDAMB231 cell invasion *in vitro*.

USP19 overexpression enhances migration and invasion

In order to complement our analysis on the putative role of USP19 as a positive regulator of migration and invasion, we analyzed the effect of USP19 overexpression in a poorly migratory and non-invasive breast cancer cell line (MCF7).

For this purpose, we stably transfected MCF7 cells with a USP19 overexpressing plasmid (Fig. 4A), and then performed wound healing assays. As shown in Figure 4B, USP19 overexpression induced a significant increase in the gap covered area, compared to the control cell line.

As a control, we overexpressed a catalytically mutant version of USP19, and in contrast to USP19 wild type, we did not detect an increase in migration compared to the control cell line.

This result further supports the hypothesis that USP19 is a positive regulator of migration, and it provides evidence that this phenotype is dependent on its catalytic activity.

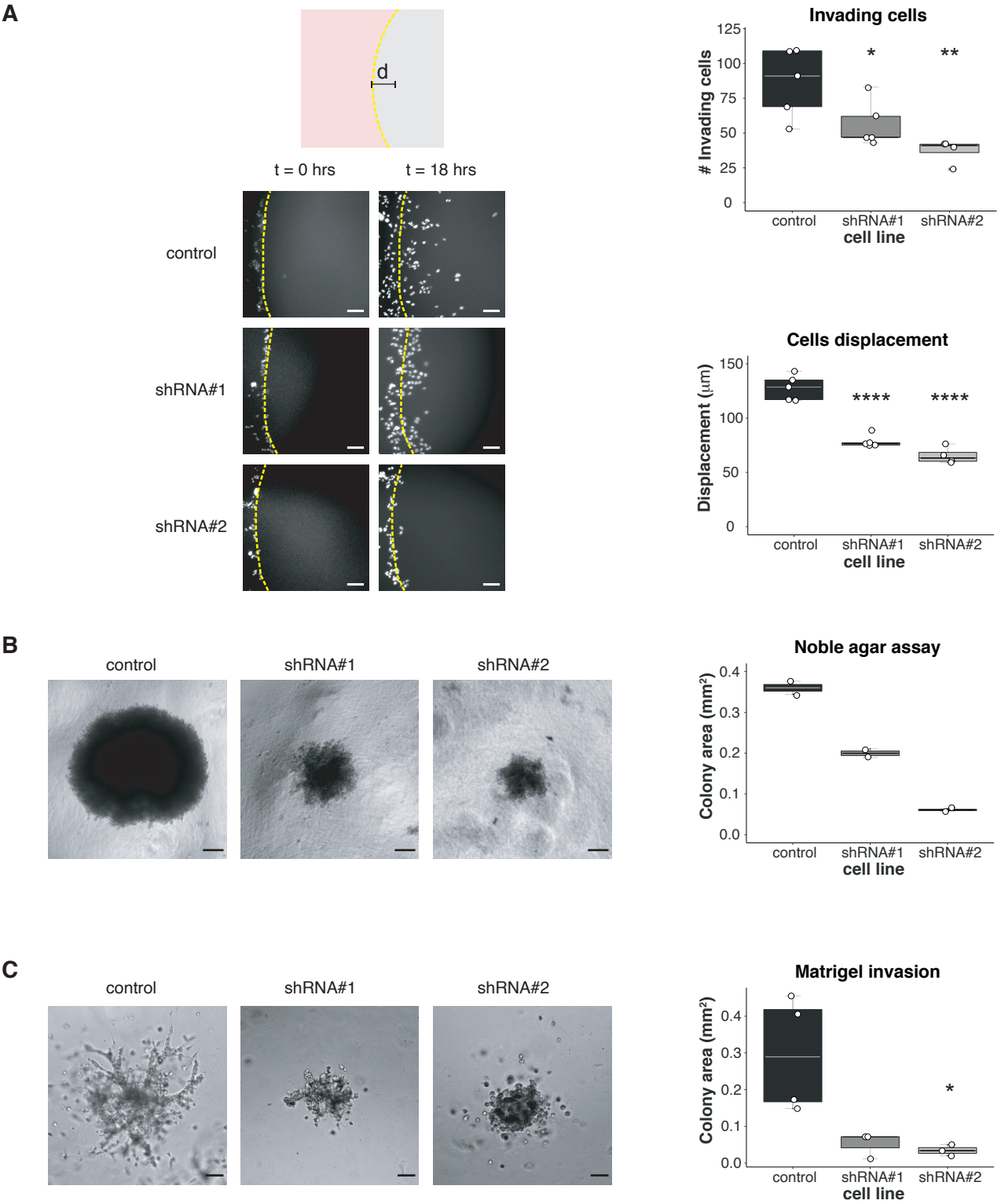

Figure 3l USP19 knockdown reduces cellular invasion.

(**A**) Top left: Diagram of agar spot assay. Cells were seeded in wells (pink surface) with drops of solidified agar (gray sphere) and allowed to invade along the bottom surface under the agar. Pictures were taken along the edge (the edge is indicated by a dotted line); the displacement (d) is the extent of invasion under agar from the spot edge until the end of the experiment. Bottom Left: Representative area showing cell invasion into an agar spot at the indicate time points. Top right: Quantification of the mean number of invading cells per spot (n≥ 4, one-way ANOVA, Dunnett's multiple comparison test. shRNA#1 p= 0.0497 and shRNA#2 p= 0.0042) and bottom right: cells mean displacement after

18 hours (n≥ 4, one-way ANOVA, Dunnett's multiple comparison test. shRNA#1 p< 0.0001 and shRNA#2 p< 0.0001). Scale bar= 100 µm. (**B**) Noble agar assay was used to study 3D culture proliferation and invasion. Left: Representative brightfield images obtained at 6 weeks in culture are shown. Scale bar= 150 µm. Right: Colony size was calculated at the end of the experiment (n= 2). (**C**) Left: Representative area showing cell invasion in a Matrigel 3D experiment after 5 days in culture. Right: Colony area was calculated at the end of the experiment (n≥ 3, Kruskal-Wallis, Dunn's multiple comparison test. shRNA#1 p= 0.1033 and shRNA#2 p= 0.0348). Scale bar= 150 µm.

Next, we analyzed the effect of USP19 overexpression on invasion and growth into a reconstituted extracellular matrix (Matrigel®), using similar experimental settings as described before. We observed a significant increase in colony areas when comparing wild type USP19 overexpressing cells to the control cell line (Fig. 4C). In accordance with our previous results, the USP19-dependent increase in invasion is also determined by its catalytic activity (Fig. 4C).

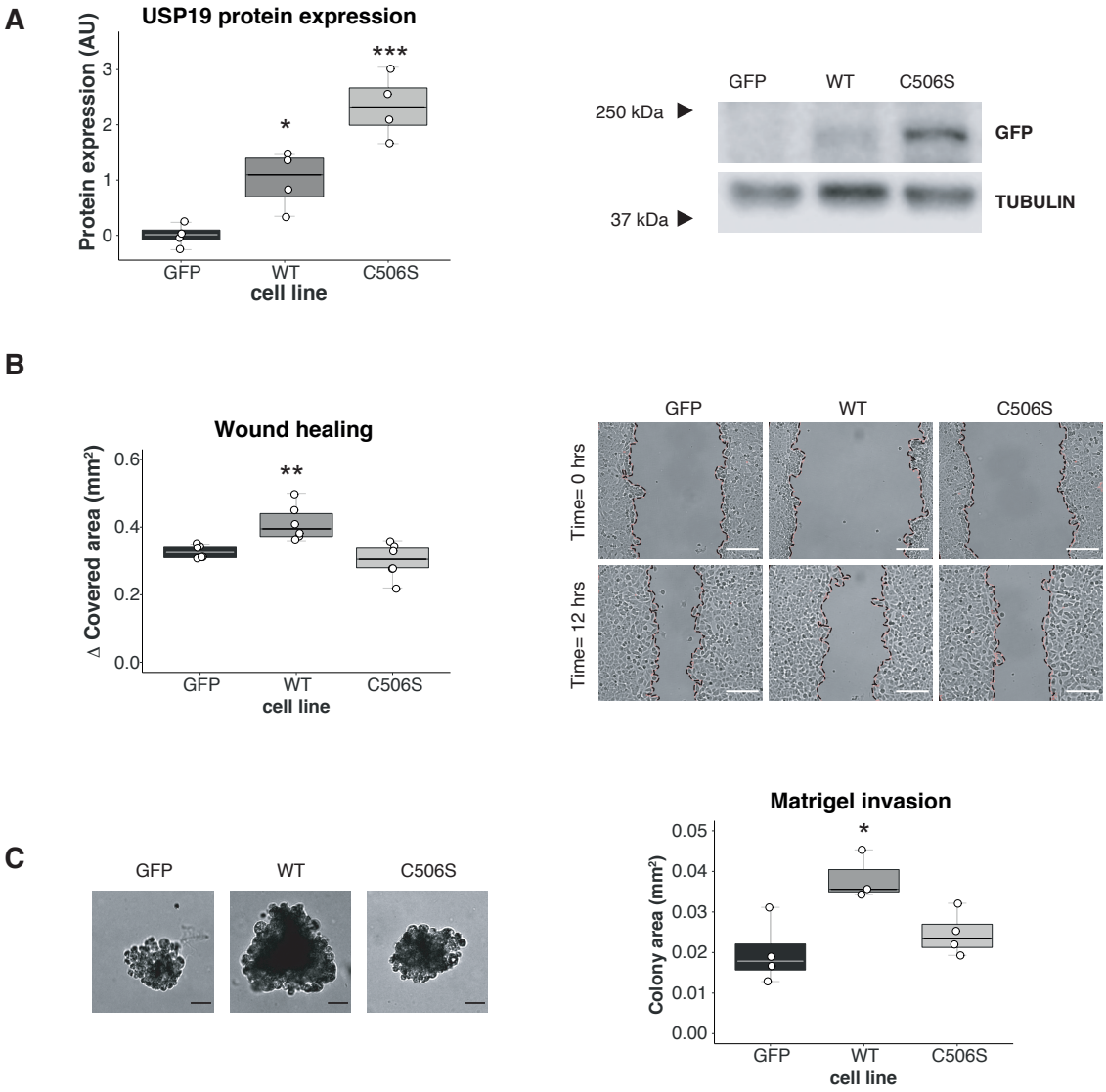

Figure 4l USP19 wild Type overexpression enhances migration and invasion in MCF7 cells.

(**A**) Different constructs of USP19 were overexpressed in MCF7 cells, and their expression confirmed by Western Blotting (n= 4, one-way ANOVA, Dunnett's multiple comparison test. WT p= 0.0269 and C506S p= 0.0001). (**B**) Migratory potential was evaluated by wound healing assay. Left: gap covered area (mm²) after 12 hours (n= 6, one-way ANOVA, Dunnett's multiple comparison test. WT p= 0.0089 and C506S p= 0.5343) and right: representative areas in a wound healing experiment at the indicated time points. Scale bar= 100 µm. (**C**) Matrigel invasion was assessed over a 30 days period. Left: Representative brightfield images obtained at the end of the experiment using a 10X objective are shown; scale bar= 50 µm. Right: colony size was calculated (n≥ 3, Kruskal-Wallis, Dunn's multiple comparison test. WT p= 0.0154 and C506S p= 0.5728).

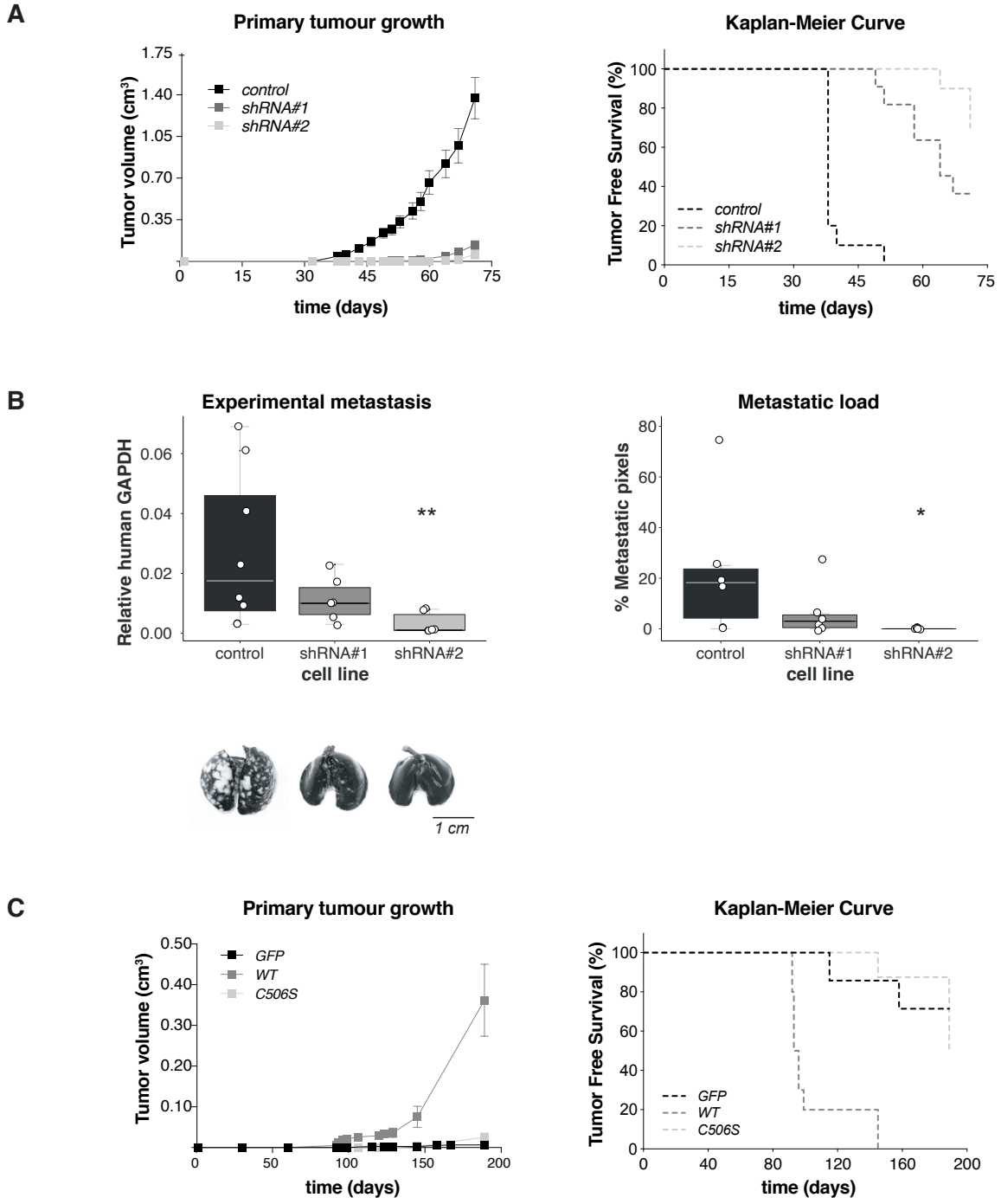

Figure 5l Analysis of USP19 expression relevance using mice models.

(**A**) Downregulation of USP19 attenuates tumorigenicity *in vivo*: Control or USP19-silenced MDAMB231 cells were subcutaneously inoculated into the mammary fat pads of female NOD/SCID mice and tumor growth monitored every 2-3 days. Left: tumor volume was calculated at the indicated time points (results show mean value ± S.E.); right: Kaplan-Meier curves were built for Tumor Free Survival (TFS) over time ($n \geq 10$, Log-Rank (Mantel-Cox) test, shRNA#1 $p < 0.0001$ and shRNA#2 $p < 0.0001$). (**B**) Silencing effects of USP19 on experimental metastasis assays: NOD/SCID male mice were inoculated with MDAMB231 USP19-silenced cells through tail vein injection and after 2 months, lungs were harvested. Top left: metastatic foci were estimated by qPCR human DNA quantification ($n \geq 6$, Kruskal-Wallis, Dunn's multiple comparison test. shRNA#1 $p > 0.9999$ and shRNA#2 $p = 0.0032$). Bottom left: representative lung images stained with Indian ink at the end of the experiment are shown. Scale bar= 1 cm. Right: metastatic load quantification was performed by evaluating lung Hematoxylin & Eosin stained slides. We used a lesion-based analysis of percent of metastatic pixels to compare the differences in metastatic load produced on the lungs by the MDAMB231 cell lines ($n = 6$, Kruskal-Wallis, Dunn's multiple comparison test. shRNA#1 $p > 0.9999$ and shRNA#2 $p = 0.0299$). (**C**) USP19 catalytic activity is needed for tumorigenicity *in vivo*: control, WT or C506S mutant versions of USP19 overexpressing MCF7 cells were subcutaneously inoculated into the mammary fat pads of female NOD/SCID mice. Left: tumor volume was calculated at the indicated time points (results show mean value ± S.E.); right: Kaplan-Meier curves were built for Tumor Free Survival (TFS) over time ($n \geq 7$, Log-Rank (Mantel-Cox) test, WT $p < 0.0001$ and C506S $p = 0.5307$).

USP19 regulates invasion *in vivo*

To further characterize USP19-dependent control of cell invasion *in vivo*, we performed subcutaneous orthotopic xenotransplants and experimental metastasis assays in immunocompromised mice (NOD/SCID).

First, we injected MDAMB231 control or USP19-silenced cells subcutaneously in the mammary fat pad of female mice and monitored tumor growth every 2-3 days. Tumor growth curves analysis indicated that those generated from MDAMB231 control cells were significantly more volumetric than the ones originated from USP19-silenced cells (Fig. 5A, left and Supp. Fig. 3). Moreover, Kaplan-Meier curves for tumor-free survival indicated that cells expressing either of the shRNAs targeting USP19 generated fewer tumors compared to the control cell line (Fig. 5A, right and Supp. Table 1). In addition, we observed similar results using another breast cancer cell line (Supp. Fig. 4 and Supp. Table 1).

Second, we analyzed USP19's role in the regulation of tumor cell lung colonization. For that purpose, we inoculated control or USP19-silenced MDAMB231 cells through tail vein injection and harvested the lungs two months later. As shown in Figure 5B, USP19 depletion inhibits tumor foci formation *in vivo*, as evaluated by human DNA quantification (left) and metastatic load quantification in Hematoxylin & Eosin stained lung sections (right). We observed the same trend when another breast cancer cell line was used (Supp. Fig. 4).

Last, we repeated the same type of tests using MCF7 cells in similar experimental conditions. We subcutaneously injected control cells or cells expressing either wild type or catalytically mutant versions of USP19 in female mice.

In agreement with our *in vitro* experiments, wild type USP19-expressing cells formed tumors in all injected mice, whereas mice injected with cells expressing the catalytic mutant did not show signs of tumor growth (Fig. 5C, Supp. Fig. 3 and Supp. Table 1). This latter observation is consistent with the fact that the MCF7 cell line does not usually form tumors unless an external estrogen source is supplied, highlighting the importance of USP19 for tumor development and onset.

Altogether, we concluded that USP19 is important for *in vivo* colonization and tumor growth. In addition, our results indicate that USP19 catalytic activity is required for its stimulatory effect on cell motility.

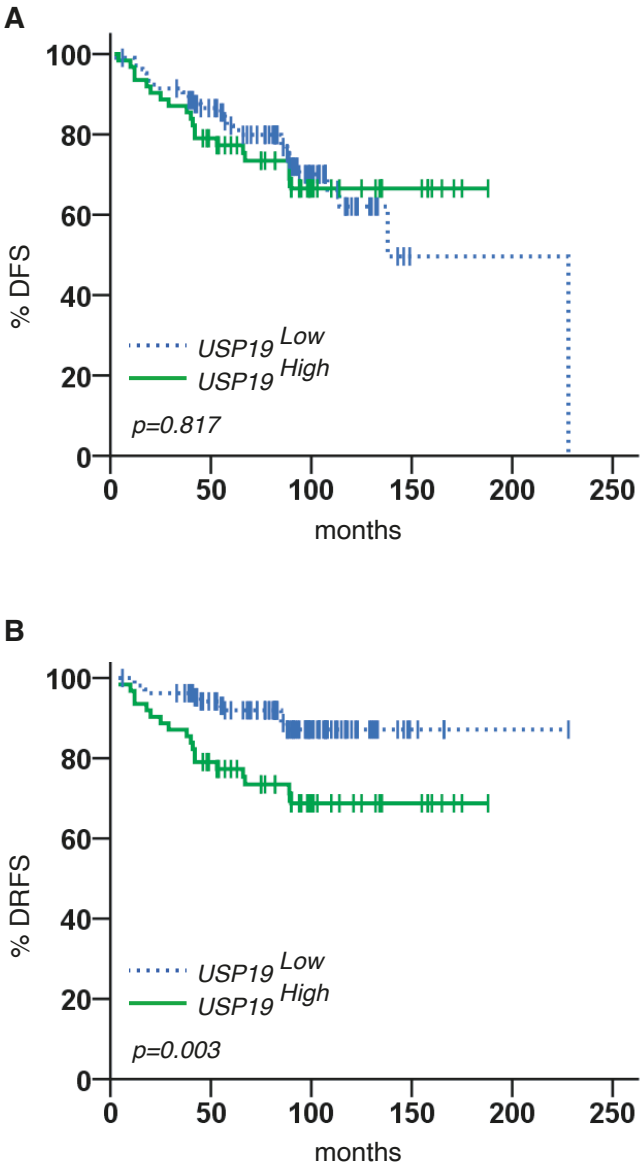

Figure 6I Prognostic value of USP19 protein expression in breast cancer patients.

Kaplan-Meier estimates of disease free survival (DFS) and distant relapse free survival (DRFS) in patients with early breast cancer tumors, according to high (solid green lines) and low (dashed blue lines) expression of USP19. (**A**) 19 out of 62 patients (30.6%) harboring USP19^{High} tumors and 30 out of 106 patients (28.3%) with USP19^{Low} tumors had a disease relapse (n= 168, Log-Rank (Mantel-Cox) test, p= 0.817). (**B**) Distant metastases developed in 18 out of 62 (29.0%) and 11 out of 106 (10.4%) of patients with USP19^{High} and USP19^{Low} tumors, respectively (n= 168, Log-Rank (Mantel-Cox) test, p= 0.003).

Survival analysis of USP19 expression in early breast cancer patients

Finally, we analyzed USP19 protein expression in a cohort study of early breast cancer patients (T1-2, N0, M0; n= 168) with long-term follow-up. Kaplan-Meier plots showed that overexpression of USP19 was associated with a significantly higher frequency of distant relapse (distant relapse free survival, DRFS), while no significant correlation with disease free survival (DFS) was observed (Fig. 6A and B).

Multivariate analysis of DRFS, adjusted for other prognostic factors, revealed that USP19^{High} was an independent prognostic predictor of DRFS (Table 1).

Altogether these findings indicate that USP19 is a new predictor of distant metastasis formation in early breast cancer patients.

Variable	HR	95% CI	P*
Disease-free survival			
Tumor size, cm (>2 *vs* ≤ 2)	1.0	0.6-1.9	0.888
Tumor grade (1 *vs* 2-3)	1.1	0.5-2.8	0.793
ER (negative *vs* positive)	1.6	0.6-4.2	0.302
PR (negative *vs* positive)	1.1	0.5-2.6	0.853
Ki-67 (positive *vs* negative)	1.1	0.6-2.0	0.818
HER-2 (positive *vs* negative)	1.9	0.9-4.2	0.112
USP19 (low *vs* high)	1.0	0.6-1.9	0.926
Distant Relapse-Free Survival			
Tumor size, cm (≤ 2 *vs* >2)	1.4	0.6-3.1	0.413
Tumor grade (2-3 *vs* 1)	3.6	0.5-27.0	0.221
ER (negative *vs* positive)	2.7	0.9-8.8	0.090
PR (positive *vs* negative)	1.8	0.6-5.3	0.313
Ki-67 (positive *vs* negative)	1.1	0.5-2.4	0.808
HER-2 (positive *vs* negative)	1.9	0.8-4.6	0.176
USP19 (high *vs* low)	2.4	1.1-5.4	0.032*

Table 1| USP19^{High} is an independent prognostic predictor of DRFS.

Multivariate analysis of USP19 expression in breast tumors. HR: Hazard Ratio, CI: Confidence Interval (n= 168, Cox's proportional hazard model, DFS p= 0.926, DRFS p= 0.032).

DISCUSSION

Migration occurs in a wide variety of physiological conditions, and alterations in its regulation are associated with different pathologies, including cancer [2, 3, 32]. In this disease, mortality is associated primarily with tumor growth at secondary sites, and effective therapies to block the metastatic cascade are lacking [6]. Tumor cells need to migrate, invade and colonize new niches prior to metastasis, making it a vital trait of malignancy. Indeed, a recent work indicated that migration, rather than proliferation, is strongly associated with breast cancer patient survival [33]. Therefore, modulation of genes that regulate migration and invasion could find application for the treatment of cancer. In line with this reasoning, we chose to screen for genes that positively regulate motility within the UPS, as this cascade is currently emerging as an attractive therapeutic target in drug development [34-37]. Here we report the identification of USP19, a deubiquitinating enzyme, as a positive regulator of migration. USP19 was initially characterized as a DUB predominantly localized in the cytosol in association with Hsp90 and other chaperones [28]. USP19 has been associated with the regulation of the half-life of several proteins that participate in different cellular processes [29, 38-50]. To our knowledge, it has not been associated with migration or invasion yet.

Our *in vitro* validation experiments showed that USP19 depletion did not affect cell proliferation in agreement with Lu *et al.* [51], but directly inhibited cellular migration. In addition, we observed that USP19 knockdown impaired invasion, as evaluated by agar drop assays and three-dimensional basement membrane cultures (Figs. 2, 3 and Supp. Fig. 2). When we analyzed growth into noble agar, the size of the resulting colonies was smaller than control cells, indicating that USP19 silencing also reduced anchorage-independent growth (Fig. 3). In all cases, we observed a correlation between the extent of USP19 silencing and the reduction of migration and invasion potential. These results are in agreement with USP19-silencing deleterious effects in growth and development in Zebrafish embryos [52].

To further confirm our results, we analyzed how USP19 overexpression affected migration and invasion, using a poorly migratory cell line. In agreement with our depletion experiments, USP19 overexpression induced an increase in cellular migration, invasion and growth in three-dimensional basement membrane cultures. These effects were dependent on the presence of a highly conserved cysteine at the catalytic site and mutation of this residue abolished USP19-induced migration and

invasion. Taken together, these *in vitro* results suggest that USP19 expression levels are associated with the regulation of motility, invasion, and anchorage-independent growth in breast cancer cell lines.

Our *in vivo* studies using immunocompromised mice demonstrated that USP19 silencing decreased cell engraftment and tumor growth, as well as colonization into the lungs (Fig. 5A and Supp. Fig. 4B). On the contrary, overexpression of wild type USP19, but not its catalytically deficient mutant version, promoted tumor growth (Fig. 5B). This is compatible with the requirement of USP19 catalytic activity for local invasion and growth in three dimensions, both *in vitro* and *in vivo*.

Finally, a retrospective study conducted on human breast tumor samples indicated that high USP19 protein levels are associated with high-risk for metastatic relapse in patients diagnosed with early breast cancer (Fig. 6).

Altogether these results provide evidence indicating that USP19 has great potential as a therapeutic target for drug development in breast cancer treatment.

In this regard, there is considerable scientific evidence demonstrating that DUBs exhibit strong substrate selectivity, which can be advantageous to ensure high efficacy and low adverse effects. Moreover, the design and development of a selective enzyme inhibitor is easier than generating an enzyme activator due to competitive inhibition and modeling of substrates [53]. In fact, numerous inhibitors for DUB activities have been already identified [54-58]. All this evidence indicates that drug development to inhibit USP19 activity is plausible. Indeed, an orally bioavailable compound has been developed, but it yet remains to be pre-clinically tested for the treatment of cancer [59].

USP19 molecular mechanism of action in the regulation of migration and invasion remains to be determined. USP19 could either affect migration and invasion directly, or alternatively, it could induce an invasive mesenchymal-like phenotype, both compatible with the observed aggressive behavior in tumor growth and invasion.

Supporting the latter, we analyzed e-cadherin protein expression levels in the same breast cancer samples described before and observed an inverse correlation between USP19 and e-cadherin expression (n= 168, Spearman correlation analysis, rho= -0.180, p= 0.032). In agreement with our results, previous reports demonstrated that low e-cadherin expression holds a prognostic value as a predictor of poorer prognosis and more aggressive phenotypes in breast cancer [60, 61]. Moreover, we performed an *in silico* analysis on breast cancer mRNA expression publicly available datasets, which revealed that high USP19 expression levels correlate with the activation of the Wnt pathway (Supp. Fig. 7). This is consistent with a recent work which showed that USP19 regulates LRP6 stability, a co-receptor of the Wnt signaling cascade [44]. Aberrant activation of this pathway is associated with cancer, and it correlates with poor prognosis and metastasis development in breast cancer [62-65]. On the other hand, USP19 was identified as a putative regulator of the transforming growth factor-β (TGF-β) type I receptor (TβRI) stability [66], whose deregulation is associated with numerous pathologies, including breast cancer [67-72].

For all the reasons expressed before, we conclude that USP19 is relevant for the regulation of breast cancer cell dissemination and its expression levels correlate with high risk of metastases development, and therefore it could represent a novel target for the management of breast cancer metastatic disease.

ACKNOWLEDGEMENTS

This work was supported by grants from the Agencia Nacional de Promoción Científica y Tecnológica (ANPCyT) PICT 2011-2783, PICT2016-2620 and PICT 2018-03688 awarded to MR. JEM was supported by NIH R01CA117907, NIH R01GM120109, NSF MCB-1817582 and NIH P30CA046934 grants, and GS was funded by an AIRC grant: IG2016 id18467. FAR and JHES are postdoctoral fellows of Consejo Nacional de Investigaciones Científicas y Técnicas (CONICET), and EHCR was recipient from a fellowship from Instituto Nacional del Cáncer (INC).

AUTHOR CONTRIBUTIONS

FAR conceived, designed, and administered the study; acquired, interpreted, and analyzed data, and wrote the manuscript with assistance from JHES and MR. JHES and EHCR were responsible for acquisition, analysis, and interpretation of data.

MJ prepared the shRNA library. AP processed screen sequencing data. MAC performed *in silico* pathway activation analysis. BD and GS performed mouse tissue staining, measurements, and data analysis. SB, VDL, GS and RL performed patients' biopsies staining, data collection and analysis. JEM provided resources, helped in funding acquisition and coordinated the NGS sequencing and analysis processes. MR conceptualized, designed, supervised, and administered the study, reviewed the manuscript, and acquired financial support for the project leading this publication.

MATERIALS AND METHODS

Cell lines and cell culture

The human breast cancer cell lines MCF7, MDAMB231 and MDAMB436 and the Hek293T cells were obtained from the ATCC and cultured in Dulbecco's modified Eagle's medium (DMEM) (Gibco) supplemented with 10% fetal bovine serum (FBS) (Natocor, Córdoba, Argentina), 50U/ml penicillin-streptomycin and 200μM L-glutamine at 37°C and 5% CO_2 in a humidified incubator. ATCC uses morphology, karyotyping, and PCR based approaches to confirm the identity of human cell lines. Mycoplasm contamination was evaluated monthly by PCR, and cell lines were cultured less than three months.

shRNA screening and plasmid transfections

A pool of plasmids encoding 1,885 shRNAs targeting 407 different genes related to the ubiquitination pathway (UB/DUB library) in the pLKO.1 backbone produced by The RNAi Consortium (TRC, Sigma-Aldrich, St. Louis, MO) were obtained from the University of Colorado Cancer Center Functional Genomics Shared Resource. 1 mg of the shRNA library plasmid DNA at 100 ng/mL was mixed with 4 mg of packaging plasmid mix (pD8.9 and pCMV-VSVG lentiviral packaging plasmids at a 1:1 ratio) and incubated with 30 mg of polyethylenimine for 15 min at RT. The entire mixture was then added to a 100 mm dish containing Hek293T packaging cells at 75% confluence. 6 hours after transfection, media on cells was replaced with complete DMEM and 48 hours after media replacement, the supernatant from each dish of packaging cells (now containing lentiviral library particles) was filtered through 0.45 mm cellulose acetate filters and stored at -80ºC until use. Before performing the screen, MOI determination of the lentivirus stock was carried out using different dilutions. Target cells were seeded at $8x10^4$ cells/well in 6-well plates and then transduced with the lentivirus. After 48 hours the infective media was removed, and target cells were selected for 5 days with a 0.5 µg/ml puromycin DMEM medium. The amount of virus required to maintain 10% survival was used. These infection conditions were essential for each cell to be transduced with less than one lentivirus particle expressing a single shRNA. Target cells were transduced with a 1:27 dilution of the lentivirus stock and were then combined at the time of harvest to reach a starting number of $4,4x10^6$ cells per condition (~300X coverage of the library complexity). 48 hours after transduction, the media was replaced with puromycin selection media and cells were then propagated for 14 days before use, in order to select out those shRNA targeting essential genes.

For single shRNA transduction, SHC001, TRCN0000051715 and TRCN0000051716 PLKO.1 vectors were used (obtained from the University of Colorado Cancer Center Functional Genomics Shared Resource); no MOI determination was performed.

For overexpression experiments, transfections were performed using Lipofectamine 2000 reagent (Invitrogen, Carlsbad, CA) according to the manufacturer's protocol. GFP tagged USP19 plasmids were a kind gift of Dr. Sylvie Urbé (University of Liverpool, UK).

Transwell migration assay

All cell lines were starved during 24 hours in assay medium (growth medium containing 0.1% FBS). The starved cells were trypsinized, $5x10^4$ cells were added to the top chamber of 24-well transwells (8 µm pore size membrane; BD Bioscience, Bedford, MA), and assay medium was added to the bottom chambers and incubated for 24 hours. After non-migratory cells removal, membranes were fixed, stained with 4′,6-diamidino-2-phenylindole, and mounted. The whole membrane was then imaged using a Zeiss Axio Observer Z1 Inverted Epi-fluorescence microscope with montage function. Image analysis was performed with Fiji software, using an automated analysis macro to measure the number of nuclei per transwell.

For the migration screen, $6.6x10^5$ starved MDAMB231 cells expressing the shRNA library (or control cell line) were plated onto 6-well transwell chambers (8 µm pore size membrane; BD Bioscience, Bedford, MA) in assay medium. After a 24-hour incubation, the non-migratory cells were collected from the upper chamber, propagated and allowed to re-migrate eleven times for enrichment purposes (the non-migratory cells of each migration experiment were used for the subsequent cycle of enrichment). The non-migratory cells of 8 transwells were combined per each selection cycle to ensure a > 700 library coverage. Simultaneously, the percentage of non-migratory cells in each cycle was determined in 24-well plates as described before, using 8 µm pore size membrane transwells (BD Bioscience, Bedford, MA).

shRNA library preparation and sequencing

The library preparation strategy uses genomic DNA and two rounds of PCR in order to isolate the shRNA cassette and prepare a single strand of the hairpin for sequencing by means of an XhoI restriction digest in the stem-loop region. We used barcoded half-hairpin sequences for the identification of shRNAs from every enrichment cycle. The procedure was performed as described previously [73]. After purity analysis of the sequencing library, barcode adaptors were linked to each sample to allow a multiplexing strategy. A HiSEQ 2500 HT Mode V4 Chemistry Illumina instrument was used for that purpose and each sample was quantified and mixed together at a final concentration of 10 ng/mL. Samples were sequenced with a simple 1x50 run and on average $1.2x10^6$ reads were obtained per sample (> 600X shRNA library complexity).

shRNA screen analysis

shRNA data were analyzed in a similar fashion to RNA-seq data. Briefly, quality control was performed with FastQC, reads were trimmed to include only shRNA sequences using FASTQ trimmer and filtered with the FASTQ Quality Filter. Reads were then aligned to a custom reference library of shRNA sequences using TopHat2.

Quantitative PCR

Total RNA was extracted from cell lines using TRIzol reagent (Invitrogen, Thermo Fisher Scientific) according to the manufacturer's instructions and complementary DNA synthesis was carried out using M-MLV reverse transcriptase in the presence of RNasin RNase inhibitor (Promega) and an oligo(dT) primer (Invitrogen).

Total DNA was extracted from cell lines or fixed tissues using Qiagen DNeasy Blood and Tissue kit with the optional RNAse A treatment step and following the manufacturer's instructions.

Quantitative real-time PCR amplification, using specific primer sets at a final concentration of 300 nM, was carried out using the FastStart Essential DNA Green Master kit (Roche) at an annealing temperature of 60°C for 35 cycles, and a CFX96 PCR Detection System (Biorad). Expression was calculated for each gene by the comparative CT (ΔCT) method with GAPDH for normalization.

Sequences and expected product sizes are as follows:

Usp19 sense 5′-*CAAATGTTCTCATCGTGCAGCTC*-3′, antisense 5′-*CTTGCTCAGGTCCAGGTTCCTAACA*-3′ (110 bp) and GAPDH sense 5'-*TGCACCACCAACTGCTTAGC*-3′, antisense 5′-*GGCATGGACTGTGGTCATGAG*-3′ (87 bp) for mRNA expression analysis. (PCR primers are all intron spanning).

Human GAPDH sense 5′-*TACTAGCGGTTTTACGGGCG*-3′, antisense 5′-*TCGAACAGGAGGAGCAGAGAGCGA*-3′ (166 bp) and mouse GAPDH sense 5'-*CCTGGCGATGGCTCGCACTT* -3′, antisense 5′-*ATGCCACCGACCCCGAGGAA* -3′ (232 bp) for DNA expression analysis.

Western blot analysis

Cells were lysed in lysis buffer (50 mM Tris-HCl pH 7.4, 250 mM NaCl, 25 mM NaF, 2 mM EDTA, 0.1% Triton-X, with protease inhibitors mix (Complete ULTRA, Roche), 1 mM 1,4-DTT, 1 µM NaOV, 10 nM okadeic acid. Protein concentrations in cell lysates were determined using the BCA assay Kit (Pierce) and then prepared for loading in Laemmli buffer 4X (200 mM Tris-HCl pH 6.8, 8% m/v SDS, 40% glycerol, 50 mM EDTA, 4% v/v β-mercaptoethanol and 0.08% w/v bromophenol blue). Equal amounts of protein were separated by 8-12% SDS-PAGE and transferred to PVDF

membranes (Millipore-Merck). Membranes were incubated with primary antibodies (rabbit anti-USP19 antibody (Bethyl Cat# A301-587A, 1:2000 dilution), mouse anti-tubulin antibody (Santa Cruz Biotechnology, Cat# sc-398103, 1:3000 dilution)) and HRP-conjugated secondary antibodies (anti-rabbit: GE Healthcare Cat# NA934; anti-mouse: GE Healthcare Cat# NA931, 1:5000 dilution), and then detected using an ECL SuperSignal West Femto y West Pico detection kit (Pierce).

Crystal violet proliferation assay

$1x10^4$ cells were seeded in 96-well plates at time= 0 hours in quadruple. Every 24 hours, medium was removed at each time point, cells were rinsed with 1X PBS and fixed with methanol for 15 minutes. After 4 days, all wells were staining simultaneously with 150 µl of a 0.05% crystal violet solution for 15 minutes. Plates were then rinsed with water, dried out and the remaining crystal violet was solubilized in 150 µl methanol. The absorbance was measured at 595 nm in a plate reader.

Area-based analysis of proliferation rate

This experiment was performed as described previously, with minor modifications [74]. Briefly, $1x10^3$ cells were seeded in 96-well plates and incubated overnight to allow cell attachment. Images were then acquired under bright field illumination every 6 hours for 3 days using a 10X air objective and Zeiss Zen Blue 2011 software for image acquisition. Image analysis was performed with Fiji software, using an automated analysis macro to measure the occupied area by cells.

Wound healing assays

Cells were seeded onto 24-well culture plates at $2,5x10^5$ per well in growth medium. Confluent monolayers were starved during 24 hours in 0.1% FBS supplemented DMEM medium and a single scratch wound was created using a micropipette tip. Cells were washed with PBS to remove cell debris, supplemented with 3% DMEM medium, and incubated at 37°C under 5% CO_2 to enable migration into wounds. Images were acquired with a Zeiss Axio Observer Z1 Inverted Epi-fluorescence microscope equipped with an AxioCam HRm3digital CCD camera; a Stage Controller XY STEP SMC 2009 scanning stage and an Incubator XLmulti S1 and Heating Unit XL S1 for live imaging incubation. Images were acquired under bright field illumination every 15 minutes for 8 or 12 hours for MDAMB231 or MCF7 cells, respectively, using a 10X air objective and Zeiss Zen Blue 2011 software for image acquisition. Image analysis was performed with Fiji software, using an automated analysis macro to measure the occupied area by cells, and the results are presented as the wound covered area at the end of the experiment, relative to time= 0 hours.

Agar invasion assay

The procedure was performed as described previously, with minor modifications [75-77]. A 1% noble agar solution was heated until boiling, swirled to facilitate complete dissolution, and then taken off of the heat. When the temperature cooled to 50°C, 5 µL spots were pipetted onto 96 well cell culture plates and allowed to cool for 20 min at RT under the hood. At this point, $5x10^3$ cells were plated into spot-containing wells in the presence of 10% FCS cell culture media supplemented with 1 µg/ml Hoechst 33258 (Thermo Fisher Scientific) and allowed to adhere for 1 hour. Fluorescent images of the edges of each spot were taken every 20 minutes during 18 hours on an Axio Observer Z1 (Zeiss) Fluorescence Microscope using a 10X magnification air objective, equipped with CCD Axio Cam HRm3 digital Camera, and a XL multi S1 (D) incubation unit plus a XL S1 (D) temperature module to maintain cell culture conditions at 37°C and 5% CO_2. Acquisition was controlled with Zen Blue 2011 (Zeiss) Software. Graph construction and statistical analysis were performed using GraphPad Prism. The number and position of cells were determined using image analysis software, ImageJ/Fiji -'Trackmate' plug-in [78].

Noble agar assay

This experiment was performed as previously, with minor modifications [79]. A 2 ml mixture of 5,000 cells in assay medium and 0.3% noble agar was seeded onto a 4 ml-solidified bed of 0.6% noble agar on six-well plates. The plates were allowed to solidify and were then incubated at 37°C. The cultures were fed once a week with assay medium. The cultures were imaged, and the number of colonies was counted after 6 weeks.

Matrigel three-dimensional cell culture

Experiments were carried out based on experimental settings described before [80-83]. Briefly, 1,000 cells were cultured during the length of the experiment in 100 µl basement membrane gels composed of 9.2 µg/µl phenol red-free growth factor reduced Matrigel (BD Bioscience) in 96 well plates. 50 µl of fresh medium were added on top of each gel every three days.

Mouse tumorigenesis and metastasis models

NOD SCID mice were originally purchased from Jackson Laboratories (Bar Harbor, ME, USA), and bred in our animal facility under a pathogen-free environment. For all experiments, 7/8-week-old mice were used in accordance with protocols approved by the Institutional Board on Animal Research and Care Committee (CICUAL, Experimental Protocol # 63, 22.nov.2016), Facultad de Ciencias Exactas y Naturales (School of Exact and Natural Sciences), University of Buenos Aires.

For *in vivo* mouse tumor studies, $5x10^5$ transduced cells were suspended in 100 µl of sterile 1X PBS and subcutaneously injected in the mammary fat pads of female mice. Tumors were measured every 3 days and tumor volumes were calculated using the following formula: Vol (volume)= ½ ($width^2$ * length). Area Under Curve analysis was performed using measurements from mice that were alive at the end of the experiment.

For the experimental metastasis assay, $1x10^6$ cells were suspended in 200 µl of sterile 1X PBS and injected in the lateral tail vein of male mice. Lungs were harvested 60 days post-injection, fixed in buffered formalin and then stored in 70% ethanol until use for DNA quantification (as described before [84]) or paraffin embedding and Hematoxylin and Eosin staining, or insufflated with a 15% India Ink solution and counterstained with Fekete's solution for macrometastasis exposure and imaging.

Metastatic load quantification of lung Hematoxylin & Eosin (H&E) stained slides

The presence of tumor nodules was identified by scanning individual lung H&E stained slides with an optical microscope. Digital image files were acquired for each specimen. For the analysis of the lung metastatic area, Adobe Photoshop software was used to determine the percentage of the lung section that was occupied by the tumor. Furthermore, since the cell-surface glycoprotein CD44s is constitutively expressed by MDAMB231 cells, immunohistochemical staining with the anti-human CD44s (HCAM) antibody (clone DF1485; heat induced epitope retrieval in citrate buffer pH 6.0; dilution 1:50, incubation time: 60') was used to confirm the tumor origin of the lung nodules (Supp. Fig. 5).

In silico analysis of USP19 mRNA expression among the TCGA-BRCA dataset

Pre-processed USP19 expression levels among 800 primary breast carcinomas with intrinsic subtype data and their integrated pathway activities (pathway activity - z score of 1387 constituent PARADIGM pathways) were obtained from the TCGA Breast Cancer (BRCA) dataset at UCSC Xena browser (http://xena.ucsc.edu/). The PARADIGM algorithm integrates pathway, expression and copy number data to infer activation of pathway features within a superimposed pathway network structure extracted from NCI-PID, BioCarta, and Reactome [85].

Briefly, Luminal A/B primary breast cancer group (n= 600) was divided into low (n= 77) or high (n= 209) USP19 expression levels according to the StepMiner one-step algorithm (http://genedesk.ucsd.edu/home/public/StepMiner/). These two groups were then compared at their integrated pathway activities to identify the most relevant signaling pathways associated with USP19 expression using the SAM test ($p< 0.01$; Fold Change> 1.5) with MultiExperiment Viewer Software (MeV 4.9).

Patients and immunohistochemistry

We retrospectively extracted the eligible patients for the study from a consecutive cohort of cases (year range, 1983-2001) diagnosed with primary unilateral breast carcinoma at the Regina Elena National Cancer Institute, Rome, Italy. From the original series, only N0 patients with T1/T2 tumors were included in this study (n= 168). The patient and tumor characteristics can be found in Supplementary Tables 2 and 3. This study was reviewed and approved by the Ethics Committee of the Regina Elena National Cancer Institute, and written informed consent was obtained from all

patients. All the patients were treated with quadrantectomy and received radiation therapy, while 90 (53,6%) received chemotherapy associated or not to hormonal therapy, and 58 (34.5%) underwent only hormonal therapy. Patients with HER2-positive tumors did not receive trastuzumab because it was not available during the study period. The median follow-up was 91.5 months (range, 6 - 298 months). Follow-up data were collected from institutional records or referring physicians. During the follow-up, distant relapse was seen in 29 (17.3%) of the patients.

Tissue microarrays (TMA) were constructed by punching 2-mm-diameter cores from invasive breast carcinoma areas, as previously described [86]. TMA sections were incubated overnight with the rabbit anti-USP19 polyclonal antibody (LifeSpan, Cat# LS-C353286, 1:50 dilution) after applying the MW antigen retrieval technique at 750 W for 10 min in 10 mM Sodium Citrate Buffer (pH 6.0). The anti-rabbit EnVision kit (Agilent, CA) was used for signal amplification. For the negative control, the primary antibody was substituted with a rabbit non-immune serum.

The anti-E-cadherin mouse monoclonal antibody (clone HECD-1, 1:50 dilution, 30 min, Zymed Laboratories Inc., San Francisco, CA) was also used. Antigen retrieval was performed as described in the previous paragraph.

The immunohistochemical analysis was carried out by two pathologists (R.L., S.B.) by agreement, with both blinded to the clinicopathological information. The proportion of USP19-positive cells that showed cytosolic positivity was in the range of 4-100%, with a mean ± S.E. of 63.2% ± 3.6. E-cadherin positivity was defined as a membrane-associated, linear pattern of immunoreactivity which decorated the cell membrane entirely.

The immunohistochemical results for the estrogen receptor (ER), progesterone receptor (PR), Ki67, and HER2 status were obtained from the patient hospital records.

Statistical analysis

Results are presented as Box-and-whisker plots with median interquartile ranges plus minimum to maximum. *n* indicates the number of independent biological replicates. The one-way ANOVA with Dunnett's multiple-comparison test as well as non-parametric Kruskal-Wallis and Dunn's Tests were used to compare treatments to their corresponding control, and adjusted p-values are indicated. P-value differences of < 0.05(*), < 0.01(**), < 0.001(***) or < 0.0001(****) were considered statistically significant. GraphPad Prism and SPSS (SPSS version 15.0, Chicago, IL) statistical software were used for the analysis.

The expression of the USP19 protein in patients' samples was reported as percent of positive cells and dichotomized (high vs. low) according to the ROC analysis. The optimal cut-off parameter for USP19 positive expression was 50%. Consequently, tumors were identified as $USP19^{High}$ (n= 62) with a score above the cut-off threshold, while it was $USP19^{Low}$ (n= 106) with a score below the threshold (Supp. Fig. 6). Pearson's χ^2 or Fisher's exact tests were used to assess the relations between the tumor USP19 protein expression and the patient clinicopathological parameters. Disease-free survival (DFS) was defined as the interval from surgery to the first of the following events: tumor relapse at local or distant sites. Distant relapse-free survival (DRFS) was defined as the time from surgery to the occurrence of distant relapse. The Log-Rank (Mantel-Cox) test was used to analyze differences between the survival curves, and Cox's proportional hazard model was used to evaluate the association of USP19 expression with survival time, using covariates. The following covariates were computed in the multivariate model: tumor size, tumor grade, and ER, PR, Ki-67, HER2, and USP19 status.

BIBLIOGRAPHY

[1] Trepat X, Chen Z, Jacobson K. Cell migration. Compr Physiol 2012;2:2369-92.

[2] Acloque H, Adams MS, Fishwick K, Bronner-Fraser M, Nieto MA. Epithelial-mesenchymal transitions: the importance of changing cell state in development and disease. The Journal of clinical investigation 2009;119:1438-49.

[3] Yang J, Weinberg RA. Epithelial-mesenchymal transition: at the crossroads of development and tumor metastasis. Dev Cell 2008;14:818-29.

[4] Vicente-Manzanares M, Horwitz AR. Cell migration: an overview. Methods Mol Biol 2011;769:1-24.

[5] Hanahan D, Weinberg RA. Hallmarks of cancer: the next generation. Cell 2011;144:646-74.

[6] Gupta GP, Massague J. Cancer metastasis: building a framework. Cell 2006;127:679-95.

[7] Lefranc F, Brotchi J, Kiss R. Possible future issues in the treatment of glioblastomas: special emphasis on cell migration and the resistance of migrating glioblastoma cells to apoptosis. J Clin Oncol 2005;23:2411-22.

[8] Megalizzi V, Mathieu V, Mijatovic T, Gailly P, Debeir O, De Neve N, et al. 4-IBP, a sigma1 receptor agonist, decreases the migration of human cancer cells, including glioblastoma cells, in vitro and sensitizes them in vitro and in vivo to cytotoxic insults of proapoptotic and proautophagic drugs. Neoplasia 2007;9:358-69.

[9] Wells A, Grahovac J, Wheeler S, Ma B, Lauffenburger D. Targeting tumor cell motility as a strategy against invasion and metastasis. Trends Pharmacol Sci 2013;34:283-9.

[10] Palmer T, Ashby W, Lewis J, Zijlstra A. Targeting tumor cell motility to prevent metastasis. Adv Drug Deliv Rev 2012;63:568-81.

[11] Eckhardt BL, Francis PA, Parker BS, Anderson RL. Strategies for the discovery and development of therapies for metastatic breast cancer. Nature reviews Drug discovery 2012;11:479-97.

[12] Husnjak K, Dikic I. Ubiquitin-Binding Proteins: Decoders of Ubiquitin-Mediated Cellular Functions. Annual Review of Biochemistry 2012;81:291-322.

[13] Pickart CM. Mechanisms underlying ubiquitination. Annual Review of Biochemistry 2001;70:503-33.

[14] Nijman SMB, Luna-Vargas MPA, Velds A, Brummelkamp TR, Dirac AMG, Sixma TK, et al. A genomic and functional inventory of deubiquitinating enzymes. Cell 2005;123:773-86.

[15] Schaefer A, Nethe M, Hordijk PL. Ubiquitin links to cytoskeletal dynamics, cell adhesion and migration. The Biochemical journal 2012;442:13-25.

[16] Mohr S, Bakal C, Perrimon N. Genomic screening with RNAi: results and challenges. Annu Rev Biochem 2010;79:37-64.

[17] Ryan AASaTE. RNAi Screening for the Discovery of Novel Modulators of Human Disease. Current Pharmaceutical Biotechnology 2010:735-56.

[18] Mullenders J, Bernards R. Loss-of-function genetic screens as a tool to improve the diagnosis and treatment of cancer. Oncogene 2009;28:4409-20.

[19] So RWL, Chung SW, Lau HHC, Watts JJ, Gaudette E, Al-Azzawi ZAM, et al. Application of CRISPR genetic screens to investigate neurological diseases. Mol Neurodegener 2019;14:41.

[20] Gerhards NM, Rottenberg S. New tools for old drugs: Functional genetic screens to optimize current chemotherapy. Drug Resist Updat 2018;36:30-46.

[21] Yao H, He G, Yan S, Chen C, Song L, Rosol TJ, et al. Triple-negative breast cancer: is there a treatment on the horizon? Oncotarget 2017;8:1913-24.

[22] Garrido-Castro AC, Lin NU, Polyak K. Insights into Molecular Classifications of Triple-Negative Breast Cancer: Improving Patient Selection for Treatment. Cancer Discov 2019;9:176-98.

[23] Lee KL, Kuo YC, Ho YS, Huang YH. Triple-Negative Breast Cancer: Current Understanding and Future Therapeutic Breakthrough Targeting Cancer Stemness. Cancers (Basel) 2019;11.

[24] Mehanna J, Haddad FG, Eid R, Lambertini M, Kourie HR. Triple-negative breast cancer: current perspective on the evolving therapeutic landscape. Int J Womens Health 2019;11:431-7.

[25] Hassink GC, Zhao B, Sompallae R, Altun M, Gastaldello S, Zinin NV, et al. The ER-resident ubiquitin-specific protease 19 participates in the UPR and rescues ERAD substrates. EMBO Rep 2009;10:755-61.

[26] Lee JG, Kim W, Gygi S, Ye Y. Characterization of the deubiquitinating activity of USP19 and its role in endoplasmic reticulum-associated degradation. The Journal of biological chemistry 2014;289:3510-7.

[27] Wiles B, Miao M, Coyne E, Larose L, Cybulsky AV, Wing SS. USP19 deubiquitinating enzyme inhibits muscle cell differentiation by suppressing unfolded-protein response signaling. Molecular biology of the cell 2015;26:913-23.

[28] He WT, Xue W, Gao YG, Hong JY, Yue HW, Jiang LL, et al. HSP90 recognizes the N-terminus of huntingtin involved in regulation of huntingtin aggregation by USP19. Sci Rep 2017;7:14797.

[29] He WT, Zheng XM, Zhang YH, Gao YG, Song AX, van der Goot FG, et al. Cytoplasmic Ubiquitin-Specific Protease 19 (USP19) Modulates Aggregation of Polyglutamine-Expanded Ataxin-3 and Huntingtin through the HSP90 Chaperone. PLoS One 2016;11:e0147515.

[30] Hanahan D, Weinberg RA. Biological hallmarks of cancer. 9th ed: Wiley Blackwell; 2017.

[31] Welch DR, Hurst DR. Defining the Hallmarks of Metastasis. Cancer Res 2019;79:3011-27.

[32] Yamaguchi H, Condeelis J. Regulation of the actin cytoskeleton in cancer cell migration and invasion. Biochimica et biophysica acta 2007;1773:642-52.

[33] Nair NU, Das A, Rogkoti VM, Fokkelman M, Marcotte R, de Jong CG, et al. Migration rather than proliferation transcriptomic signatures are strongly associated with breast cancer patient survival. Sci Rep 2019;9:10989.

[34] Weathington NM, Mallampalli RK. Emerging therapies targeting the ubiquitin proteasome system in cancer. The Journal of clinical investigation 2014;124:6-12.

[35] Veggiani G, Gerpe MCR, Sidhu SS, Zhang W. Emerging drug development technologies targeting ubiquitination for cancer therapeutics. Pharmacol Ther 2019;199:139-54.

[36] Morrow JK, Lin H-K, Sun S-C, Zhang S. Targeting ubiquitination for cancer therapies. Future Medicinal Chemistry 2015;7:2333–50.

[37] Huang X, Dixit VM. Drugging the undruggables: exploring the ubiquitin system for drug development. Cell Research 2016;26:484-98.

[38] Cui J, Jin S, Wang RF. The BECN1-USP19 axis plays a role in the crosstalk between autophagy and antiviral immune responses. Autophagy 2016;12:1210-1.

[39] Gu Z, Shi W, Zhang L, Hu Z, Xu C. USP19 suppresses cellular type I interferon signaling by targeting TRAF3 for deubiquitination. Future Medicine 2017.

[40] Lei CQ, Wu X, Zhong X, Jiang L, Zhong B, Shu HB. USP19 Inhibits TNF-alpha- and IL-1beta-Triggered NF-kappaB Activation by Deubiquitinating TAK1. J Immunol 2019;203:259-68.

[41] Lim K-H, Choi J-H, Park J-H, Cho H-J, Park J-J, Lee E-J, et al. Ubiquitin specific protease 19 involved in transcriptional repression of retinoic acid receptor by stabilizing CORO2A. Oncotarget 2016;7:34759-72.

[42] Mei Y, Hahn AA, Hu S, Yang X. The USP19 deubiquitinase regulates the stability of c-IAP1 and c-IAP2. The Journal of biological chemistry 2011;286:35380-7.

[43] Nakamura N, Harada K, Kato M, Hirose S. Ubiquitin-specific protease 19 regulates the stability of the E3 ubiquitin ligase MARCH6. Experimental cell research 2014;328:207-16.

[44] Perrody E, Abrami L, Feldman M, Kunz B, Urbe S, van der Goot FG. Ubiquitin-dependent folding of the Wnt signaling coreceptor LRP6. eLife 2016;5.

[45] Wu X, Lei C, Xia T, Zhong X, Yang Q, Shu HB. Regulation of TRIF-mediated innate immune response by K27-linked polyubiquitination and deubiquitination. Nature communications 2019;10:4115.

[46] Altun M, Zhao B, Velasco K, Liu H, Hassink G, Paschke J, et al. Ubiquitin-specific protease 19 (USP19) regulates hypoxia-inducible factor 1alpha (HIF-1alpha) during hypoxia. The Journal of biological chemistry 2012;287:1962-9.

[47] Gierisch ME, Pedot G, Walser F, Lopez-Garcia LA, Jaaks P, Niggli FK, et al. USP19 deubiquitinates EWS-FLI1 to regulate Ewing sarcoma growth. Sci Rep 2019;9:951.

[48] Harada K, Kato M, Nakamura N. USP19-Mediated Deubiquitination Facilitates the Stabilization of HRD1 Ubiquitin Ligase. International journal of molecular sciences 2016;17.

[49] Lu Y, Adegoke OA, Nepveu A, Nakayama KI, Bedard N, Cheng D, et al. USP19 deubiquitinating enzyme supports cell proliferation by stabilizing KPC1, a ubiquitin ligase for p27Kip1. Mol Cell Biol 2009;29:547-58.

[50] Wu M, Tu H-q, Chang Y, Tan B, Wang G, Zhou J, et al. USP19 deubiquitinates HDAC1/2 to regulate DNA damage repair and control chromosomal stability. Oncotarget 2017;8:2197-208.

[51] Lu Y, Bedard N, Chevalier S, Wing SS. Identification of distinctive patterns of USP19-mediated growth regulation in normal and malignant cells. PLoS One 2011;6:e15936.

[52] Tse WK, Eisenhaber B, Ho SH, Ng Q, Eisenhaber F, Jiang YJ. Genome-wide loss-of-function analysis of deubiquitylating enzymes for zebrafish development. BMC Genomics 2009;10:637.

[53] Farshi P, Deshmukh RR, Nwankwo JO, Arkwright RT, Cvek B, Liu J, et al. Deubiquitinases (DUBs) and DUB inhibitors: a patent review. Expert Opin Ther Pat 2015;25:1191-208.

[54] Fraile JM, Quesada V, Rodriguez D, Freije JM, Lopez-Otin C. Deubiquitinases in cancer: new functions and therapeutic options. Oncogene 2012;31:2373-88.

[55] Luise C, Capra M, Donzelli M, Mazzarol G, Jodice MG, Nuciforo P, et al. An atlas of altered expression of deubiquitinating enzymes in human cancer. PLoS ONE 2011;6.

[56] Wei R, Liu X, Yu W, Yang T, Cai W, Liu J, et al. Deubiquitinases in cancer. Oncotarget 2015;6:12872–89.

[57] D'Arcy P, Wang X, Linder S. Deubiquitinase inhibition as a cancer therapeutic strategy. Pharmacol Ther 2015;147:32-54.

[58] Poondla N, Chandrasekaran AP, Kim K-S, Ramakrishna S. Deubiquitinating enzymes as cancer biomarkers: new therapeutic opportunities? BMB Reports 2019;52:181-9.

[59] Jacq X, Gavory G, O'Dowd C, Cranston A, Baker O, Bell C, et al. Discovery and development of first-in-class orally bioavailable USP19 inhibitors [abstract]. . American Association for Cancer Research Annual Meeting 2019. Atlanta, GA. Philadelphia (PA): Cancer Res 2019 2019.

[60] Li Z, Yin S, Zhang L, Liu W, Chen B. Prognostic value of reduced E-cadherin expression in breast cancer: a meta-analysis. Oncotarget 2017;8:16445-55.

[61] Yang L, Wang XW, Zhu LP, Wang HL, Wang B, Zhao Q, et al. Significance and prognosis of epithelial-cadherin expression in invasive breast carcinoma. Oncol Lett 2018;16:1659-65.

[62] Bilir B, Kucuk O, Moreno CS. Wnt signaling blockage inhibits cell proliferation and migration, and induces apoptosis in triple-negative breast cancer cells. Journal of translational medicine 2013;11:12.

[63] Geyer FC, Lacroix-Triki M, Savage K, Arnedos M, Lambros MB, MacKay A, et al. beta-Catenin pathway activation in breast cancer is associated with triple-negative phenotype but not with CTNNB1 mutation. Modern pathology : an official journal of the United States and Canadian Academy of Pathology, Inc 2011;24:209-31.

[64] Khramtsov AI, Khramtsova GF, Tretiakova M, Huo D, Olopade OI, Goss KH. Wnt/beta-catenin pathway activation is enriched in basal-like breast cancers and predicts poor outcome. The American journal of pathology 2010;176:2911-20.

[65] Matsuda Y, Schlange T, Oakeley EJ, Boulay A, Hynes NE. WNT signaling enhances breast cancer cell motility and blockade of the WNT pathway by sFRP1 suppresses MDA-MB-231 xenograft growth. Breast Cancer Res 2009;11:R32.

[66] Zhang L, Zhou F, Drabsch Y, Gao R, Snaar-Jagalska BE, Mickanin C, et al. USP4 is regulated by AKT phosphorylation and directly deubiquitylates TGF-beta type I receptor. Nat Cell Biol 2012;14:717-26.

[67] Barcellos-Hoff MH, Akhurst RJ. Transforming growth factor-β in breast cancer: too much, too late. Breast Cancer Research;11:1-6.

[68] Morikawa M, Derynck R, Miyazono K. TGF-b and the TGF-b Family: Context-Dependent Roles in Cell and Tissue Physiology. Cold Spring Harb Perspect Biol 2016.

[69] Huang F, Chen YG. Regulation of TGF-beta receptor activity. Cell Biosci 2012;2:9.

[70] Moses H, Barcellos-Hoff MH. TGF-beta biology in mammary development and breast cancer. Cold Spring Harb Perspect Biol 2011;3:a003277.

[71] Xie F, Ling L, van Dam H, Zhou F, Zhang L. TGF-beta signaling in cancer metastasis. Acta Biochim Biophys Sin (Shanghai) 2018;50:121-32.

[72] Zarzynska JM. Two faces of TGF-beta1 in breast cancer. Mediators Inflamm 2014;2014:141747.

[73] Sullivan KD, Lewis HC, Hill AA, Pandey A, Jackson LP, Cabral JM, et al. Trisomy 21 consistently activates the interferon response. eLife 2016;5.

[74] Bahnson A, Athanassiou C, Koebler D, Qian L, Shun T, Shields D, et al. Automated measurement of cell motility and proliferation. BMC Cell Biol 2005;6:19.

[75] Wiggins H, Rappoport J. An agarose spot assay for chemotactic invasion. Biotechniques 2010;48:121-4.

[76] Salvany L, Muller J, Guccione E, Rorth P. The core and conserved role of MAL is homeostatic regulation of actin levels. Genes & development 2014;28:1048-53.

[77] Ahmed M, Basheer HA, Ayuso JM, Ahmet D, Mazzini M, Patel R, et al. Agarose Spot as a Comparative Method for in situ Analysis of Simultaneous Chemotactic Responses to Multiple Chemokines. Sci Rep 2017;7:1075.

[78] Tinevez JY, Perry N, Schindelin J, Hoopes GM, Reynolds GD, Laplantine E, et al. TrackMate: An open and extensible platform for single-particle tracking. Methods 2017;115:80-90.

[79] Rameshwar P, Patel S, Pine S, Rameshwar P. Noble Agar Assay for Self-Renewal. Protocol Exchange 2013.

[80] Ampuja M, Jokimäki R, Juuti-Uusitalo K, Rodriguez-Martinez A, Alarmo E-L, Kallioniemi A. BMP4 inhibits the proliferation of breast cancer cells and induces an MMP-dependent migratory phenotype in MDA-MB-231 cells in 3D environment. BMC Cancer 2013;13:1-13.

[81] Farias EF, Petrie K, Leibovitch B, Murtagh J, Chornet MB, Schenk T, et al. Interference with Sin3 function induces epigenetic reprogramming and differentiation in breast cancer cells. Proc Natl Acad Sci U S A 2010;107:11811-6.

[82] Ibrahim AM, Sabet S, El-Ghor AA, Kamel N, Anis SE, Morris JS, et al. Fibulin-2 is required for basement membrane integrity of mammary epithelium. Sci Rep 2018;8:14139.

[83] Sadej R, Romanska H, Baldwin G, Gkirtzimanaki K, Novitskaya V, Filer AD, et al. CD151 regulates tumorigenesis by modulating the communication between tumor cells and endothelium. Molecular cancer research : MCR 2009;7:787-98.

[84] Llorens MC, Rossi FA, Garcia IA, Cooke M, Abba MC, Lopez-Haber C, et al. PKCalpha Modulates Epithelial-to-Mesenchymal Transition and Invasiveness of Breast Cancer Cells Through ZEB1. Front Oncol 2019;9:1323.

[85] Vaske CJ, Benz SC, Sanborn JZ, Earl D, Szeto C, Zhu J, et al. Inference of patient-specific pathway activities from multi-dimensional cancer genomics data using PARADIGM. Bioinformatics 2010;26:i237-45.

[86] Lattanzio R, Marchisio M, La Sorda R, Tinari N, Falasca M, Alberti S, et al. Overexpression of activated phospholipase Cgamma1 is a risk factor for distant metastases in T1-T2, N0 breast cancer patients undergoing adjuvant chemotherapy. Int J Cancer 2013;132:1022-31.

SUPPLEMENTARY FIGURES

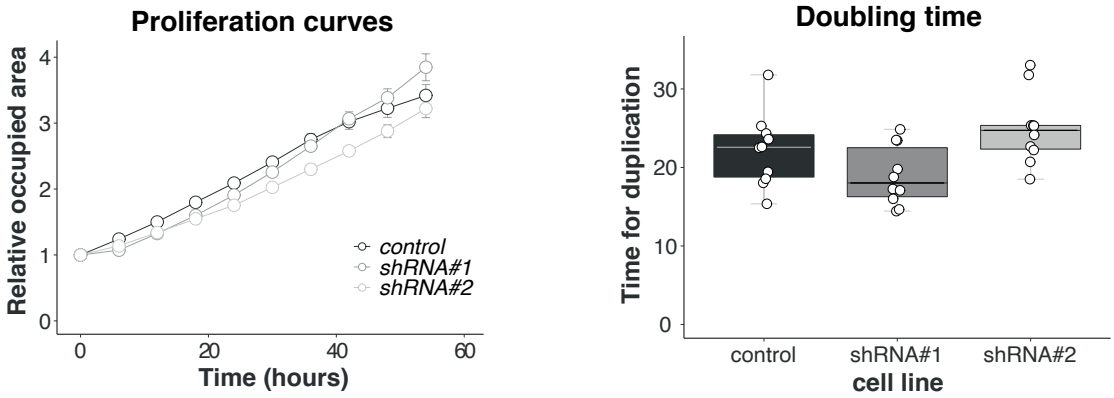

Figure S1I Doubling time of USP19 silenced MDAMB231 cells.

An area-based analysis of proliferation rate was used to determine cell growth over time. Cells were seeded onto wells, allowed to attach and imaged at the indicated time points. Left: relative mean occupied area at each time point ± S.E., and right: doubling time calculated for control and USP19 silenced cell lines (n= 10, one-way ANOVA, Dunnett's multiple comparison test. shRNA#1 p= 0.1953 and shRNA#2 p= 0.2824).

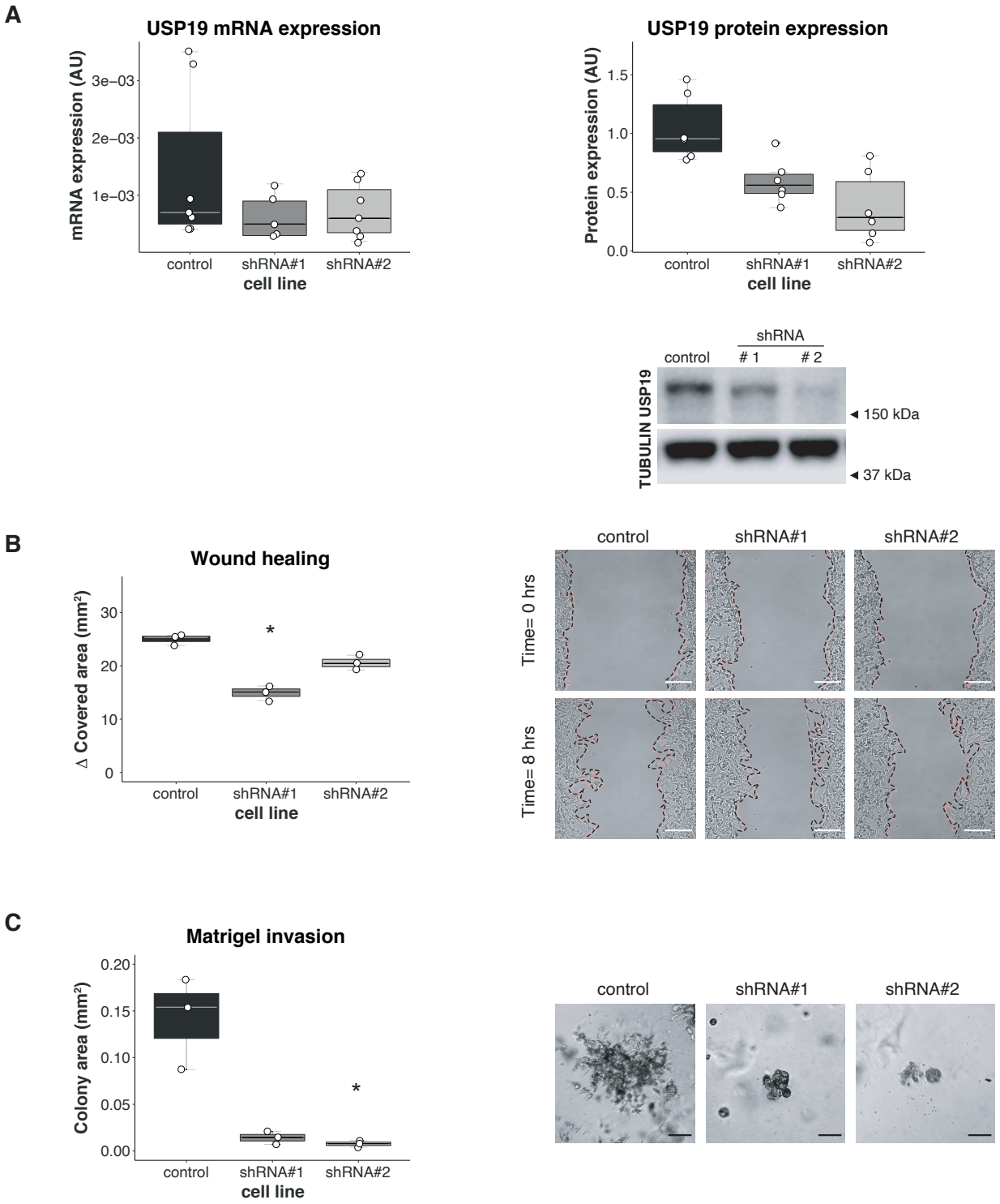

Figure S2l *in vitro* validation in MDAMB436 cells.

USP19 silencing effects were studied in MDAMB436 cells. (**A**) Left: Efficiencies of shRNA-mediated target gene knockdown were confirmed by RT-PCR (n≥ 5, Kruskal-Wallis, Dunn's multiple comparison test. shRNA#1 p= 0.6028 and shRNA#2 p= 0.8335) and Right: Western Blotting (n= 4, one-way ANOVA, Dunnett's multiple comparison test. shRNA#1 p= 0.1787 and shRNA#2 p= 0.0633). (**B**) Cells migratory potential evaluated by wound healing assay. Left: gap covered area (mm^2) after 8 hours (n= 3, Kruskal-Wallis, Dunn's multiple comparison test. shRNA#1 p= 0.0146 and shRNA#2 p= 0.3594); right: representative areas in a wound healing experiment at the indicated time points. Scale bar= 100 µm. (**C**) Invasiveness assessed with Matrigel 3D experiments. Left: Colony area was calculated at the end of the experiment (n= 3, Kruskal-Wallis, Dunn's multiple comparison test. shRNA#1 p= 0.2021 and shRNA#2 p= 0.0341); right: a representative area for the cell invasion assay after 5 days in culture is shown. Scale bar= 200 µm.

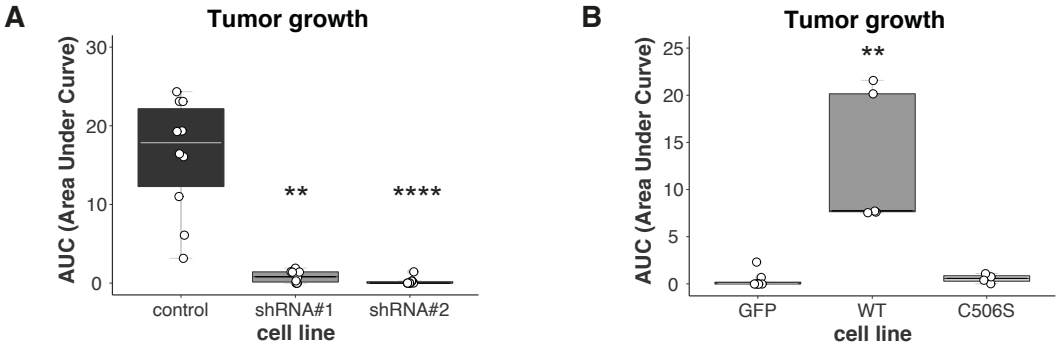

Figure S3l Tumor growth analysis.

Area Under Curve (AUC) analysis using Tumor Mean Volume curves. (**A**) AUC values of mice injected with MDAMB231 cells (n≥ 10, Kruskal-Wallis, Dunn's multiple comparison test. shRNA#1 p= 0.0021 and shRNA#2 p< 0.0001). (**B**) AUC values of mice injected with MCF7 cells (n≥ 4, Kruskal-Wallis, Dunn's multiple comparison test. WT p= 0.0015 and C506S p= 0.7582).

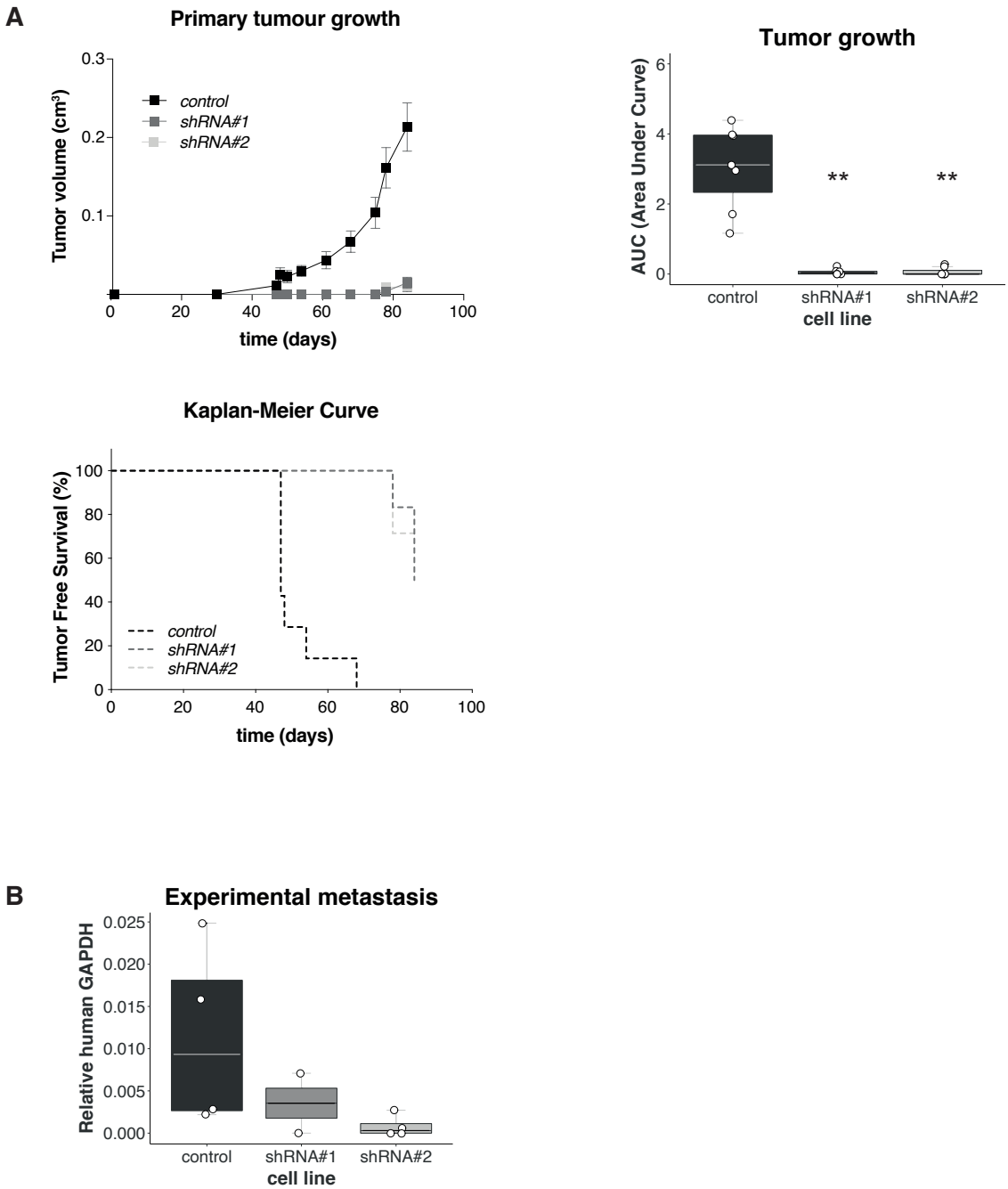

Figure S4I *In vivo* experiments with MDAMB436 cells.

(**A**) Downregulation of USP19 attenuates tumorigenicity *in vivo*: Control or USP19-silenced MDAMB436 cells were subcutaneously inoculated into the mammary fat pads of female NOD/SCID mice. Top left: Tumor volume was measured at the indicated time points (results show mean value ± S.E.). Top right: the area under the tumor volume curves was calculated at the end of the experiment (n≥ 6, Kruskal-Wallis, Dunn's multiple comparison test. shRNA#1 p= 0.0053 and shRNA#2 p= 0.0014). Bottom: Kaplan-Meier curves were built for Tumor Free Survival (TFS) over time (n≥ 6, Log-Rank (Mantel-Cox) test, shRNA#1 p= 0.0003 and shRNA#2 p= 0.0001). (**B**) Experimental metastasis assay: NOD/SCID male mice were inoculated with MDAMB436 USP19-silenced cells through tail vein injection and after 2 months, lungs were harvested. Metastasis foci were estimated by qPCR human DNA quantification (n≥ 2).

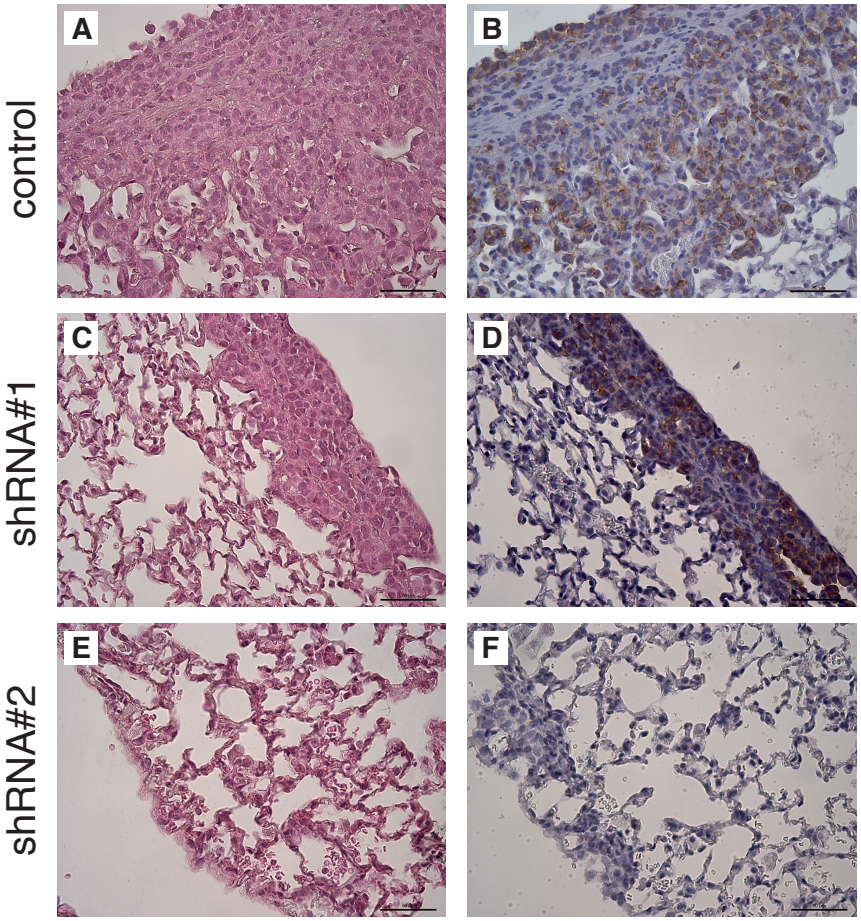

Figure S5l Metastatic load determination.

Representative images of lung sections of mice injected with control or USP19-silenced MDAMB231 cells. Tissues were analyzed for metastatic load by Hematoxylin & Eosin staining (**A**, **C**, and **E**), and nodules tumor origin was confirmed by staining with the mouse anti-human CD44s monoclonal antibody (**B**, **D**, and **F**). Scale bar: 50 µm.

A

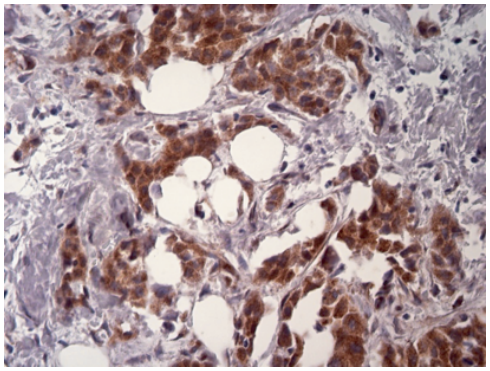

B

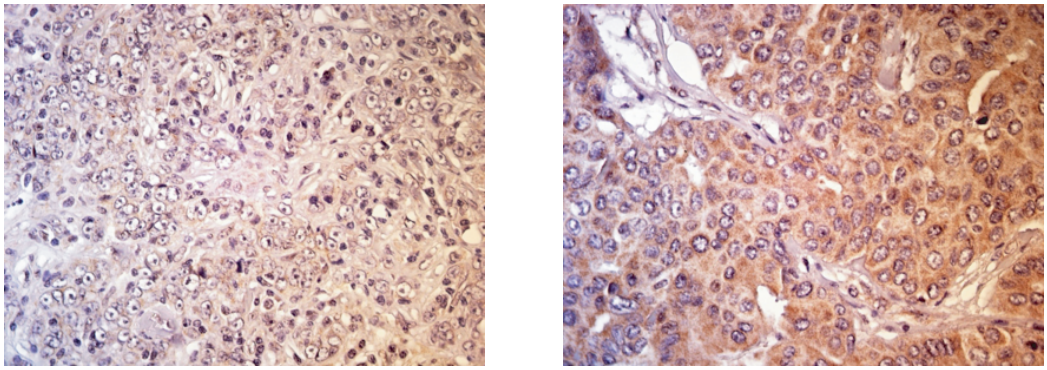

Figure S6l USP19 staining on FFPE breast cancer tissues.

(**A**) Adipose tissue invasion by ductal carcinoma cells with strong immunopositivity for USP19; the immunoreactivity is predominantly located in the cytoplasm. (**B**) Immunohistochemical staining: examples of low (left panel) and high (right panel) expression of USP19 in breast cancer (magnification X400).

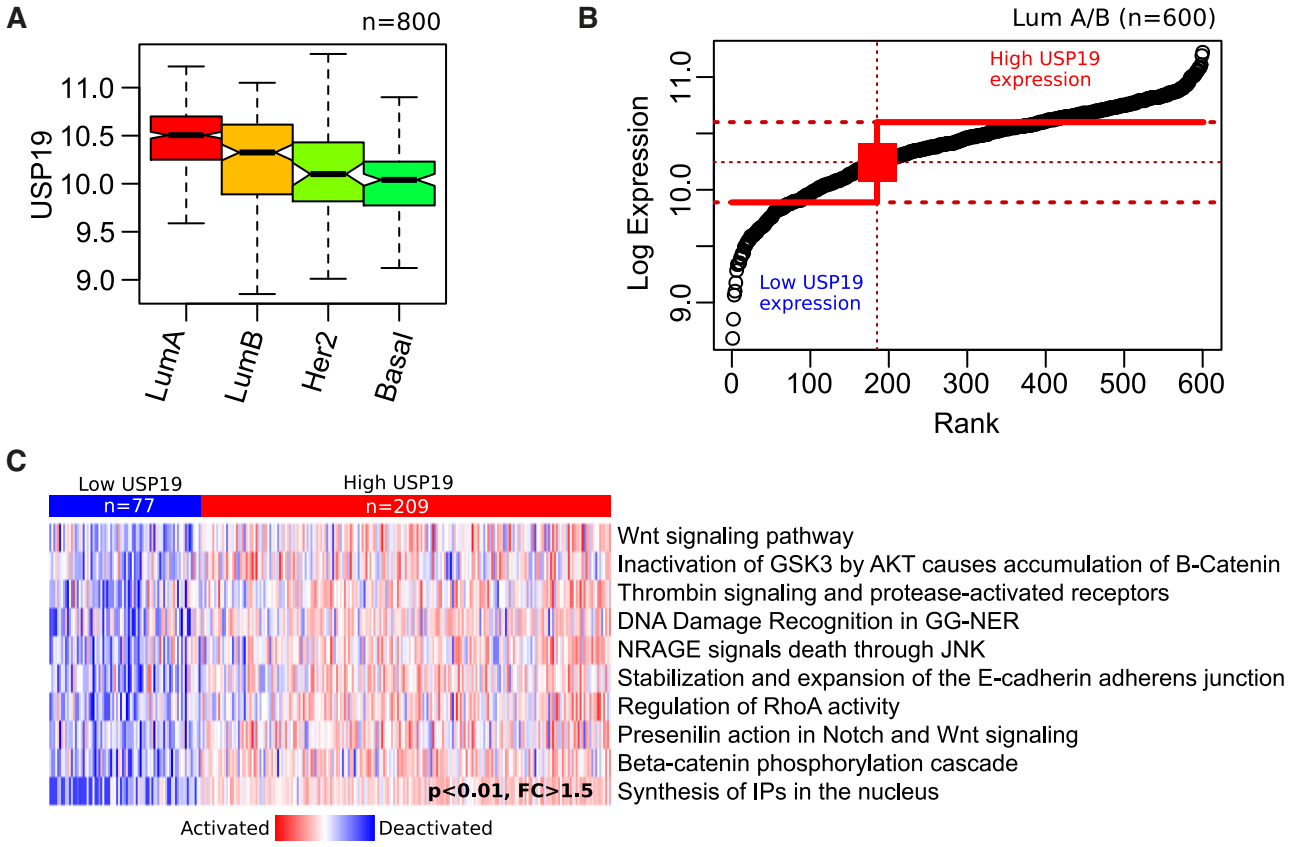

Figure S7I *In silico* study of the relationship between USP19 expression levels and different pathway activation status.

(**A**) USP19 mRNA expression among primary breast carcinomas according to their intrinsic subtype. Expression analysis showed a consistent up-regulation in luminal A and B subtypes compared with basal-like and Her2 subtypes. (**B**) Luminal A/B primary breast cancers divided into low (n= 77) or high (n= 209) USP19 mRNA expression levels. (**C**) Significantly activated pathways among Luminal A/B tumors with high USP19 mRNA expression (n≥ 77, SAM test, p< 0.01).

SUPPLEMENTARY TABLES

cell line		Tumor-free Median Survival (days)	Long-Rank (Mantel-Cox) test vs control		Hazard Ratio (logrank) vs control	
			p value	Summary	Ratio	95% CI
MDAMB231	control	38	-	-	-	-
	shRNA#1	64	<0.0001	****	4.315	1.347-12.96
	shRNA#2	undefined	<0.0001	****	6.845	2.149-21.80
MDAMB436	control	47	-	-	-	-
	shRNA#1	84	0.0003	***	5.768	1.468-22.67
	shRNA#2	undefined	0.0001	***	8.399	2.002-35.23
MCF7	GFP	undefined	-	-	-	-
	WT	94.5	0.0003	***	7.953	2.488-25.43
	C506S	189	0.6000	ns	1.536	0.305-7.719

Table S1I Analysis of Tumor Free Survival curves in USP19 silencing and overexpression *in vivo* experiments.

Median Tumor Free Survival was calculated. Long-rank test was used to analyze differences between Tumor Free Survival curves in mice injected with MDAMB231, MDAMB436 or MCF7 cells.

Variable	Value (%)
Age at diagnosis (yr)	
Median	56.7
<50	51 (30.4)
50-65	69 (41.1)
>65	48 (28.6)
Menopausal status	
Pre/perimenopausal	54 (32.1)
Postmenopausal	114 (67.9)
Molecular subtypes	
Luminal A	71 (42.3)
Luminal B	57 (33.9)
HER2 positive	8 (4.8)
Triple negative	32 (19.0)
Tumor size	
≤ 2 cm	109 (64.9)
> 2 cm	59 (35.1)
Histotypes	
Ductal carcinoma	135 (80.4)
Lobular carcinoma	24 (14.3)
Other	9 (5.3)
Tumor grade	
1	21 (12.5)
2-3	147 (87.5)
ER	
Negative	43 (25.6)
Positive	125 (74.4)
PR	
Negative	59 (35.1)
Positive	109 (64.9)
Ki-67	
Negative	90 (53.6)
Positive	78 (46.4)
HER2	
Negative	149 (88.7)
Positive	19 (11.3)
USP19	
Low	106 (63.1)
High	62 (36.9)
Patient outcome	
Without recurrence	119 (70.8)
Local recurrence	20 (11.9)
Distant recurrence	29 (17.3)

Table S2l Characterization of patients' cohort.

Patients and tumors characteristics (n= 168).

Variable	USP19		
	Low: n (%)	High: n (%)	P*
Tumor size			
≤ 2 cm	74 (69.8)	35 (56.5)	0.095
> 2 cm	32 (30.2)	27 (42.5)	
Tumor grade			
1	17 (16.0)	4 (6.5)	0.091
2-3	89 (84.0)	58 (93.5)	
ER			
Negative	27 (25.5)	16 (25.8)	1.000
Positive	79 (74.5)	46 (74.2)	
PR			
Negative	40 (37.7)	19 (30.6)	0.404
Positive	66 (62.3)	43 (69.4)	
Ki-67			
Negative	61 (57.5)	29 (46.8)	0.201
Positive	45 (42.5)	33 (53.2)	
HER2			
Negative	100 (94.3)	49 (79.0)	0.003*
Positive	6 (5.7)	13 (21.0)	
Subtype			
Luminal A	48 (67.6)	23 (32.4)	0.014*
Luminal B	31 (54.4)	26 (45.6)	
HER2	2 (25.0)	6 (75.0)	
TN	25 (63.1)	7 (36.9)	

Table S3I Characterization of USP19 protein expression in human samples.

USP19 status according to clinicopathological features of patients (n= 168, Pearson's χ^2 test).